

2023

9.16 Sat.

國際研討會



會議地點：國立臺北科技大學 材資館五樓會議廳

報名方式：112年8月1日起至8月15日止於臺博館官方

網站教育活動線上報名 (<http://www.ntm.gov.tw/>),

限80位，額滿為止。

報名費用：免費

臺灣 寶石 礦物學



國立臺灣博物館
National Taiwan Museum



國立臺北科技大學



主辦單位：國立臺灣博物館、合辦單位：國立臺北科技大學
協辦單位：國立臺灣大學地質科學研究所、國立臺灣海洋大學地球科學研究所
國立嘉義大學通識教育中心、臺灣寶石科學研究學會、天皇礦場、山益礦場

臺灣寶玉石礦物學

國際研討會議程

2023

9.16 Sat.

會議地點：國立臺北科技大學材資館五樓會議廳

| | |
|-------------|---|
| 09:00~09:20 | 報到 |
| 09:20~09:30 | 開幕與致詞 |
| 09:30~10:00 | 發表人：方建能（國立臺灣博物館典藏管理組/副研究員兼組長） 題目：寶石級蛇紋石-臺灣墨玉研究回顧與前瞻 |
| 10:00~10:30 | 發表人：余炳盛（國立臺北科技大學資源工程研究所/教授） 題目：不同分析方法應用於閃玉地球化學研究的差異比較 |
| 10:30~11:00 | 發表人：黃怡禎（江西應用科技學院光華寶石與藝術設計學院/教學副院長） 題目：網路檢索科學研究:以閃石玉為例 |
| 11:00~11:30 | 發表人：吳詩羽（吳照明寶石顧問有限公司/營運總監） 題目：臺灣閃玉貓眼的顏色成因與譜學特徵 |
| 11:30~12:00 | 綜合座談（方建能、余炳盛、黃怡禎、吳詩羽） |
| 12:00~13:00 | 休息 |
| 13:00~13:30 | 發表人：Eslam Mohammed Ali Mitwally （國立臺北科技大學資源工程研究所/博士生） 題目：臺灣花蓮瑞穗瑞欣礦和壽豐理新礦蛇紋岩中磁鐵礦包裹體的地球化學研究 |
| 13:30~14:00 | 發表人：陳惠芬（國立臺灣海洋大學地球科學研究所/教授） 題目：拉利瑪海紋石的祕密 |
| 14:00~14:30 | 發表人：陳淑娟（義守大學工業管理學系/助理教授） 題目：寶石包裹體之評估模式與應用 |
| 14:30~15:00 | 發表人：林書弘（臺灣聯合珠寶玉石鑑定中心/所長） 題目：多變量統計在寶石學上的應用-以玻隕石和黑曜岩鑑定為例 |
| 15:00~15:30 | 綜合座談（Eslam、陳惠芬、陳淑娟、林書弘） |
| 15:30~15:45 | 休息 |
| 15:45~16:15 | 發表人：李佩倫（國立嘉義大學數位學習設計與管理學系/教授） 題目：應用拉曼光譜於鈣榴石群化學成份之分析 |
| 16:15~16:45 | 發表人：宋聖榮（國立臺灣大學地質科學系/教授） 題目：用地球化學指標鑑定祖母綠的來源 |
| 16:45~17:15 | 發表人：沈錫田（美國Guild寶石研究所/專家顧問） 題目：拉曼光譜與密度泛函理論計算在紅珊瑚色素鑑別研究中的應用 |
| 17:15~17:45 | 綜合座談（李佩倫、宋聖榮、沈錫田） |
| 17:45~18:00 | 散會 |



國立臺灣博物館
National Taiwan Museum



國立臺北科技大學

主辦單位：國立臺灣博物館
協辦單位：國立臺灣大學地質科學研究所
國立嘉義大學通識教育中心、臺灣寶石科學研究學會、天長論壇、山益礦場

目錄

寶石級蛇紋石-臺灣墨玉研究回顧與前瞻

發表人：方建能（國立臺灣博物館典藏管理組/副研究員兼組長） 1

不同分析方法應用於閃玉地球化學研究的差異比較

發表人：余炳盛（國立臺北科技大學資源工程研究所/教授） 5

網路檢索科學研究：以閃石玉為例

發表人：黃怡禎（江西應用科技學院光華寶石與藝術設計學院/教學副院長）. 9

臺灣閃玉貓眼的顏色成因與譜學特徵

發表人：吳詩羽（吳照明寶石顧問有限公司/營運總監） 11

臺灣花蓮瑞穗瑞欣礦和壽豐理新礦蛇紋岩中磁鐵礦包裹體的地球化學研究

發表人：Eslam Mohammed Ali Mitwally（國立臺北科技大學資源工程研究所/博士生） 15

拉利瑪海紋石的祕密

發表人：陳惠芬（國立臺灣海洋大學地球科學研究所/教授） 25

寶石包裹體之評估模式與應用

發表人：陳淑娟（義守大學工業管理學系/助理教授） 31

多變量統計在寶石學上的應用-以玻隕石和黑曜岩鑑定為例

發表人：林書弘（臺灣聯合珠寶玉石鑑定中心/所長） 35

應用拉曼光譜於鈣榴石群化學成份之分析

發表人：李佩倫（國立嘉義大學數位學習設計與管理學系/教授） 45

用地球化學指標鑑定祖母綠的來源

發表人：宋聖榮（國立臺灣大學地質科學系/教授） 49

拉曼光譜與密度泛函理論計算在紅珊瑚色素鑑別研究中的應用

發表人：沈錫田（美國 Guild 寶石研究所/專家顧問） 53

寶石級蛇紋石-臺灣墨玉研究回顧與前瞻

方建能

國立臺灣博物館典藏管理組

E-mail : jnfang@ntm.gov.tw

摘要

臺灣產玉，花蓮豐田荖腦山出產的綠色閃玉世界聞名，所以「臺灣玉」幾乎成了綠色閃玉的代名詞。臺灣玉自 1965 年由廖學誠發現及鑑定後，使臺灣以閃玉生產及玉石加工聞名全世界，從臺灣玉發現迄今約五十餘年，近年來有關其成因、年代、熱液作用溫度與壓力、次數與板塊構造運動關聯等重要地質議題，欣見有學者提出新的論述與探討。「臺灣墨玉」之名於 2010 年被作者等人提出，主張伴隨臺灣玉共生的臺灣墨玉，是臺灣的新品種寶石礦產。從臺灣墨玉命名迄今十餘年，除基本的礦物、物化特性的少量數據發表外，相較於臺灣玉的知名度與研究質量而言，臺灣墨玉可說是仍鮮為人知與乏人研究的。

臺灣墨玉主要礦物組成除葉蛇紋石與磁鐵礦外，另含赤鐵礦、鉻鐵礦等不透光礦物及其他少量的蜥蛇紋石、鎂橄欖石、白雲石等礦物。而依照前北京大學地質系王時麒教授對蛇紋石玉以外觀顏色分類，其中對基本顏色為深淺不一的黑色系蛇紋石玉，俗稱為墨玉。「臺灣墨玉」一詞即綜合產地加俗稱而命名。

本文針對臺灣墨玉的研究回顧與前瞻，期待能引起產、官、學等多方的關注與實際投入，使臺灣墨玉成為真正具有經濟價值的臺灣新品種寶石礦產。

關鍵字：臺灣玉、臺灣墨玉、命名、葉蛇紋石、磁鐵礦

Serpentine Gemstone: The Past and Future of Taiwan Black Jade Research

Jiann-Neng Fang

Department of Collection Management, National Taiwan Museum

E-mail: jnfang@ntm.gov.tw

Abstract

Laonao Mountain, located in Fengtian Village, Hualien County in Taiwan, is world-famous for its production of green nephrite, all but allowing “Taiwan Jade” to become the substitute name for green nephrite. Taiwan Jade was discovered and identified by Hsueh-Cheng Liao back in 1965, which drove Taiwan’s production and processing of jade to fame. Since its discovery over 50 years ago, researchers have dedicated themselves to the discussion of the Taiwan Jade’s genesis, age, metasomatism conditions, and relationship to plate tectonics, and in recent years, many new ideas and discussions have been added to the debate. The term “Taiwan black Jade” was coined in 2010 by the author of this paper, who also claimed that Taiwan Black Jade, which exists in symbiosis with Taiwan Jade, is a new specimen of gemstone found in Taiwan. Since the naming of serpentine jade over ten years ago, apart from scarce data on its mineralogy and physical and chemical characteristics, the amount of research on this specimen has been rare compared with Taiwan Jade, as has been its publicity.

Taiwan Black Jade consists mainly of antigorite and magnetite, with the addition of nontransparent minerals such as hematite and chromite, as well as low amounts of lizardite, forsterite, and dolomite. In the studies of Professor Shiqi Wang, a previous researcher of Beijing University Department of Geosciences, he categorized serpentine according to appearance and color, and gave the ones whose base color consisted of multiple shades of dark colors the common name “Black Jade”. The term “Taiwan Black Jade” was then coined with reference to both its common name and locality.

This paper serves as both a review of past studies, as well as a guide for future studies regarding Taiwan Black Jade, in the hopes that we may draw the attention and investment of the industry, government, and academia and raise the economic value of this new gemstone specimen of Taiwan.

Keywords: Taiwan Jade, Taiwan Black Jade, origin of name, antigorite, magnetite

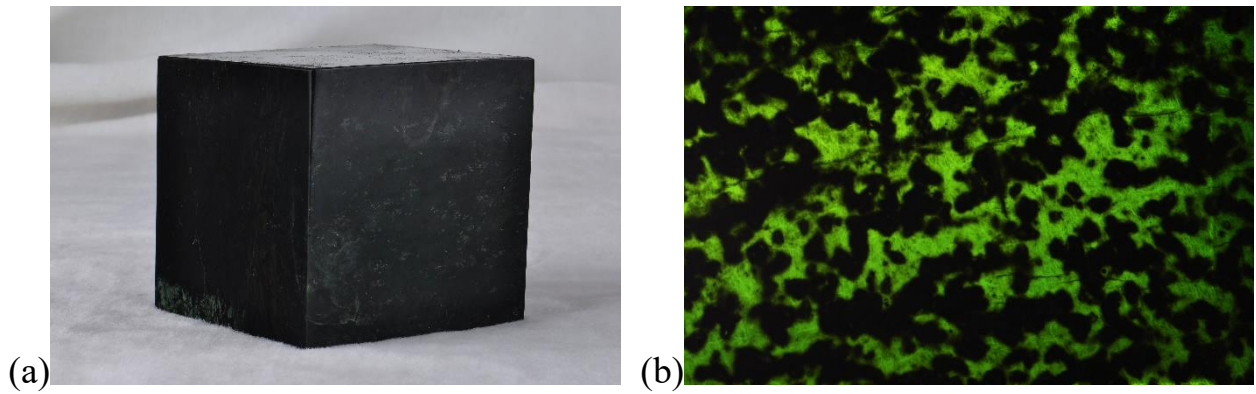


圖 1、臺灣墨玉的特性：(a)外觀為淺深不一的黑色系，(b)當厚度較薄(<2mm)且背光時局部呈半透明。

Fig. 1. The characteristics of Taiwan Black Jade: (a) the outer appearance consists of multiple shades of dark colors, and (b) partially translucent when backlit and thinner than 2 mm.

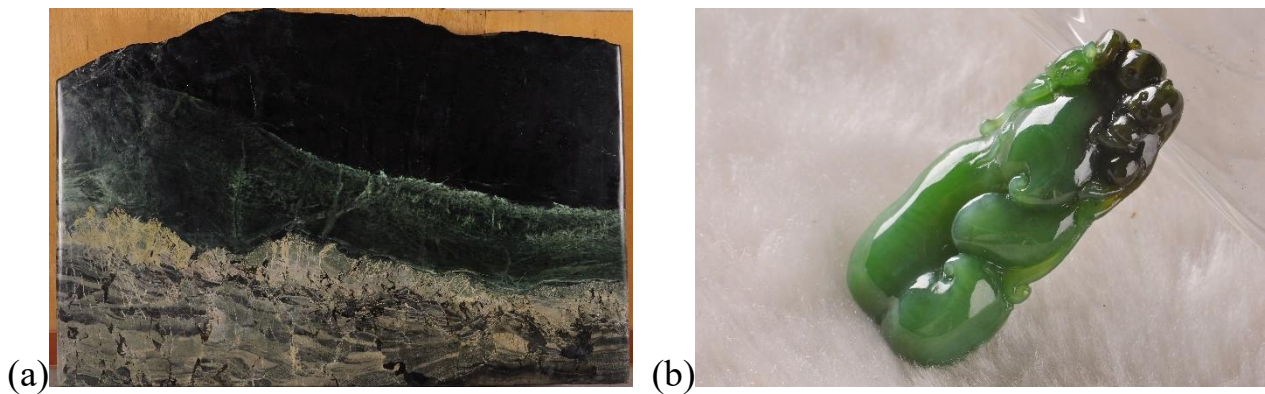


圖 2、天星礦場產出的共生臺灣玉與臺灣墨玉：(a)玉材，(b)玉飾。

Fig. 2. The symbiosis of Taiwan Jade and Taiwan Black Jade from Ten-Xin mine: (a) specimen, (b) sculpture



圖 3、天星礦場產出的臺灣墨玉之雕刻成品。

Fig. 3. The sculpture of Taiwan Black Jade from Ten-Xin mine.

表 1、臺灣墨玉拉曼光譜波峰數值

Table 1. The Raman wavenumber of Taiwan black jade samples.

| 礦物相 | 標本編號 | 波峰數值 (cm ⁻¹) | | | | | | |
|------|------|--------------------------|-------|-------|-------|-------|-------|--------|
| 葉蛇紋石 | T1-2 | - | 230vs | 376vs | - | - | 682s | 1045sh |
| 蜥蛇紋石 | T1-3 | - | 233s | 389vs | - | - | 691vs | 1100sh |
| 磁鐵礦 | T1-1 | - | - | - | - | - | 665vs | - |
| 赤鐵礦 | T1-1 | - | 225vs | 293vs | 406m | - | - | - |
| 鉻鐵礦 | T1-3 | - | - | - | - | 590s | 703vs | - |
| 鎂橄欖石 | T3-1 | - | 229sh | 304sh | 433sh | 608sh | 824vs | 857vs |
| 白雲石 | T1-4 | 175w | 299w | - | - | - | 725sh | 1097vs |

m: medium; s: strong; sh: shoulder; vs: very strong; w: weak

不同分析方法應用於閃玉地球化學研究的差異比較

余炳盛^{1*}、王奕晴²

¹ 國立臺北科技大學資源工程研究所

² 臺北市立大學地球環境暨生物資源學系

*通訊作者 E-mail: bing@ntut.edu.tw

摘要

近年來閃玉的地球化學研究被廣泛應用於成因探討及來源地鑑別等領域。而被多數學者認為較為準確的化學分析方法包含：搭配偏硼鋰酸熔融法的精密 X 光螢光法(XRF)，搭配混合酸溶法的感應耦合電漿質譜儀法(ICP-MS)，以及搭配鐳射剝蝕的感應耦合電漿質譜法(LA-ICP-MS)。本研究以採自臺灣花蓮豐田地區的 5 個閃玉標本，分別以上述三種分析方法對同一批樣品進行化學分析，嘗試瞭解不同分析方法應用於閃玉地球化學研究的差異及探討其原因。

關鍵字：地球化學、閃玉、前處理、X 光螢光法、感應耦合電漿質譜儀

Comparisons of Different Analytical Methods Applied to the Geochemical Study of Nephrite

Bing-Sheng Yu^{1*}, Yi-Ching Wang²

¹Institute of Resource Engineering, National Taipei University of Technology

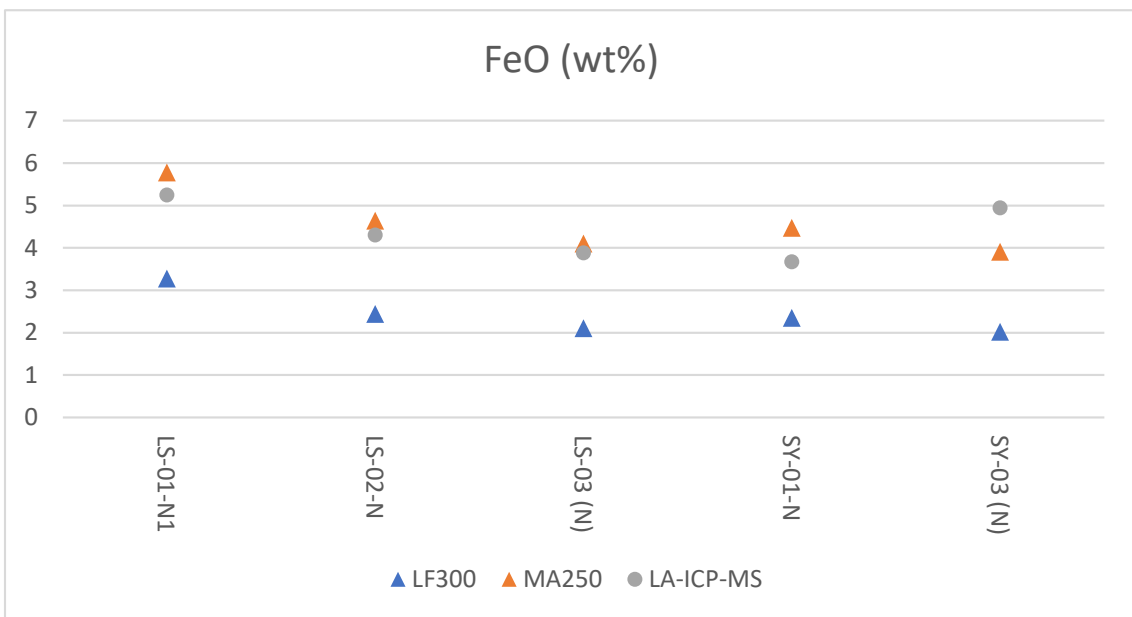
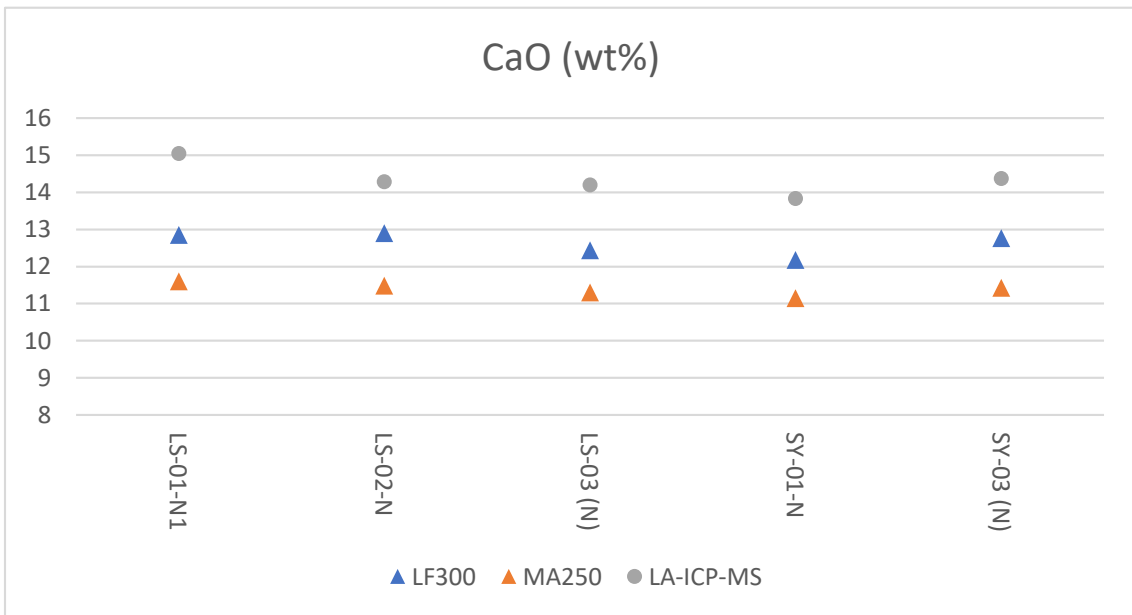
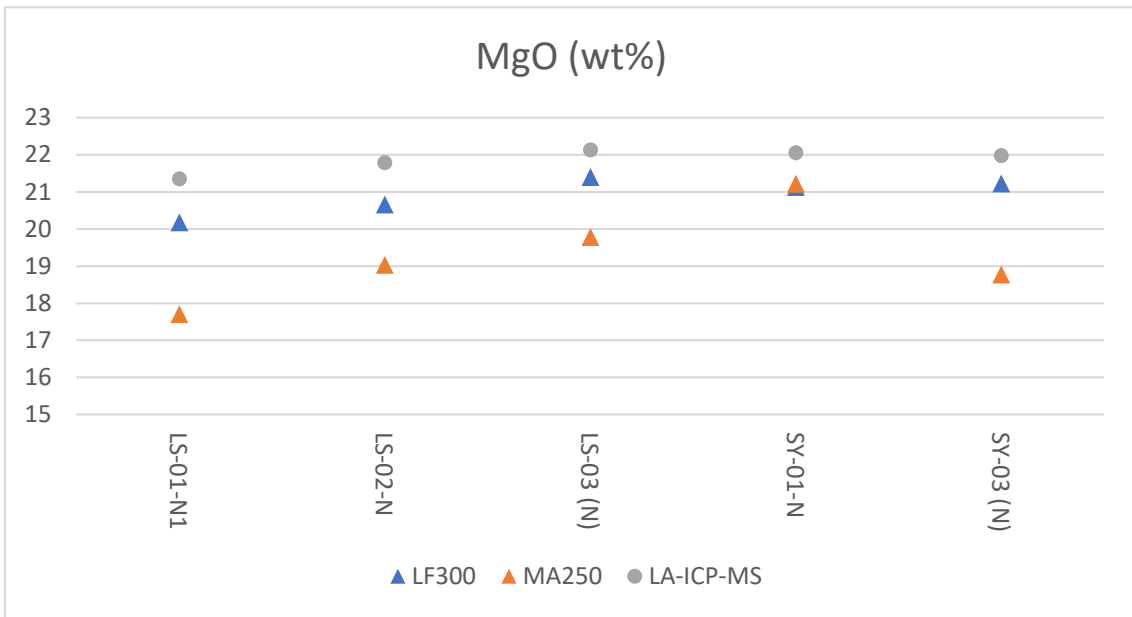
²Department of Earth and Life Science, University of Taipei

*Corresponding author, E-mail: bing@ntut.edu.tw

Abstract

Recently, the geochemical study of nephrite has been widely used in the fields of genesis exploration and source identification. The more accurate chemical analysis methods considered by most scholars include: precise X-ray fluorescence method (XRF) with pretreatment of metaborate lithium acid melting method, inductively coupled plasma mass spectrometry (ICP-MS) method with mixed acid solution pretreatment, and inductively coupled plasma mass spectrometry with laser ablation (LA-ICP-MS). In this study, a total of 5 nephrite specimens were collected from the Fengtien area of Hualien, Taiwan, and the same sample was chemically analyzed by the above three analysis methods, trying to understand the differences of these analytical methods applied to the discrepancies in the study of the geochemistry of the sapphires, and their causes.

Keywords: geochemistry, nephrite, pretreatment, X-ray fluorescence method, inductively coupled plasma mass spectrometer



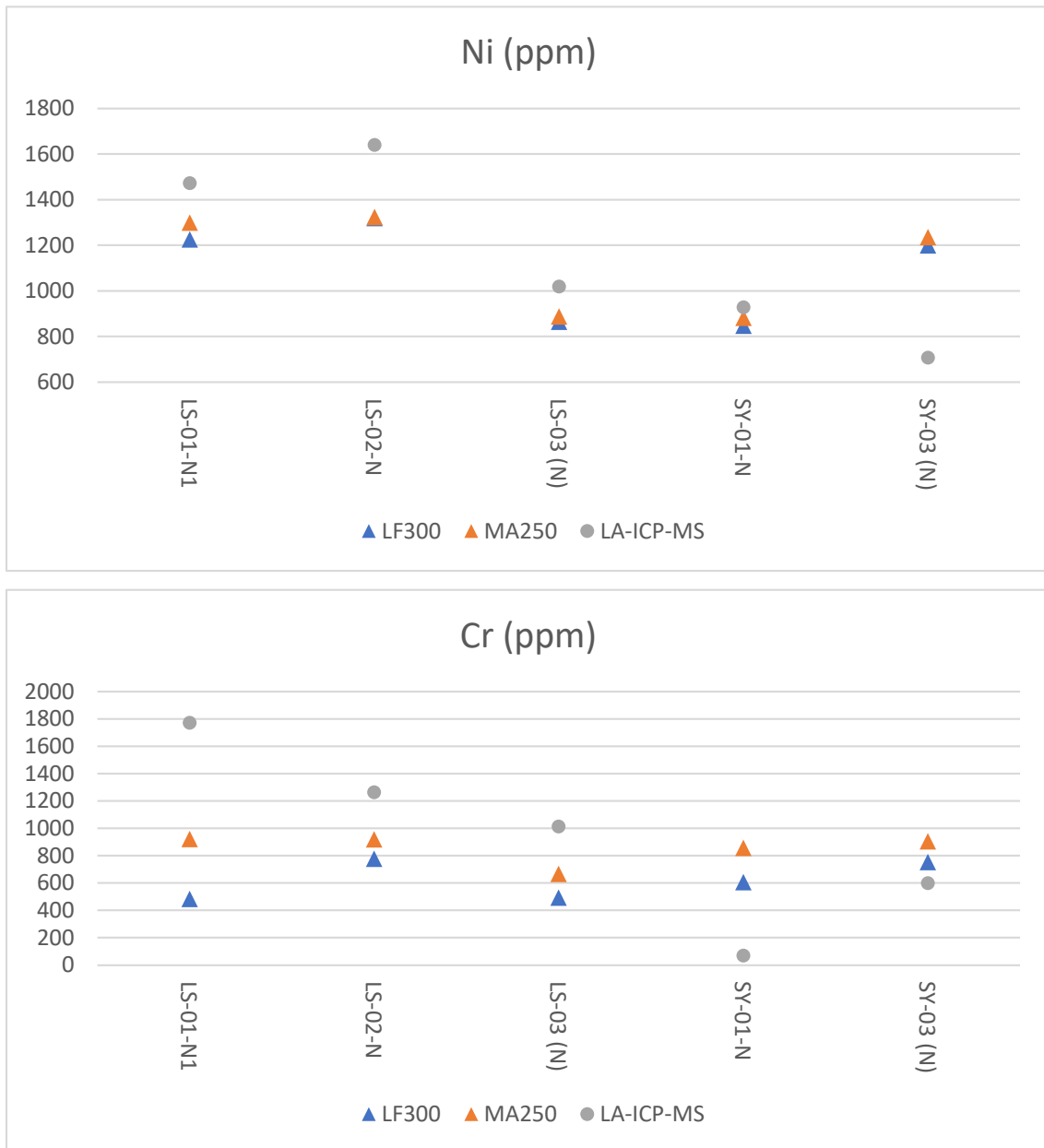


圖 1、不同分析方法對於五個閃玉樣品的分析結果比較圖

Fig. 1. Comparison of analysis results of five nephrite samples by different analysis methods

網路檢索科學研究：以閃石玉為例

黃怡禎^{1,2}

¹ 江西應用科技學院光華寶石與藝術設計學院

² 臺灣寶石科學研究學會

E-mail : eugene.huang@hpstar.ac.cn

摘要

本文通過檢索知網資料庫獲取閃石玉研究的相關的文獻，接著運用 Excel 2019、VOSviewer 等工具構建知識圖譜；結合定量與定性分析的方式開展綜合研究，嘗試釐清閃石玉的研究現狀和進展，此種文獻計量學之分析結果不僅有助於推動閃石玉科研領域的研究深度，還可以為後繼學者的相關研究提供參考。結果顯示：閃石玉研究領域主要由大學和研究性機構之 12 個研究團隊推動，研究成果集中刊發在少數主要期刊上；使用測試手段的頻次和類別整體呈穩步上升的態勢，測試手段主要有電子探針、X 射線衍射、紅外光譜等 16 種先進儀器；當前閃石玉的研究涵蓋礦床成因、成礦年代、成礦環境、礦物岩石學/寶石學特徵、產地特徵及溯源等。

關鍵字：閃石玉、知識圖譜、文獻計量學、研究項目

Bibliometric Analysis on Research Progress of Nephrite

Eugene Huang^{1,2}

¹Jiangxi University of Applied Science, School of Guanghua Gemology and Art Design, Jiangxi
330100, China

²Taiwan Gemology Research Society

E-mail : eugene.huang@hpstar.ac.cn

Abstract

Clarifying the research status and progress of nephrite not only helps to grasp the trend of research, but also provides valuable references for further research in this field. Relevant literature on nephrite was retrieved from CNKI database. Knowledge spectra was constructed by Excel 2019 and VOSviewer, and comprehensive quantitative and qualitative analyses were carried out. Results of this bibliometric analysis show that research of nephrite is mainly promoted by universities and research institutions from which 12 research teams are formed. The distribution of research results is relatively concentrated, which is mainly published in a few journals. Much progress is achieved in terms of analytical methods as well as state-of-the-art equipment. Research topics focused on nephrite genesis, chronology, metallogenic environment, mineralogical/gemological and petrological characteristics, identification of origin and locality.

Keywords: nephrite, knowledge spectra, bibliometric analysis, research topics

臺灣閃玉貓眼的顏色成因與譜學特徵

吳詩羽^{1*}、吳照明^{1,2}、江鴻源¹

¹ 吳照明寶石顧問有限公司

² 中國文化大學地質學系

*通訊作者 E-mail: jennifer.wu@fga-dga-gem.com

摘要

過往對於臺灣閃玉貓眼的研究有限，多數的研究從礦物學組成的角度探討，尚未以寶石學的角度進行顏色與成分關係的研究。

本文搜集48顆臺灣閃玉貓眼，包含不同深淺的綠色及帶有棕色及黃色色調的臺灣閃玉貓眼。採用紅外光譜儀(FTIR)、紫外近紅外光譜儀(UV-Visible-NIR)、X光螢光分析儀(XRF)及拉曼光譜儀(Raman spectroscopy)對樣品進行研究。研究結果顯示，UV-Visible-NIR下綠色臺灣閃玉貓眼隨著顏色深淺的變化，509nm的峰位有強弱上的差異，顯示樣品的綠色色調與Fe²⁺多寡有關。而具黃色或棕色色調則未有明顯509nm峰位。此外，XRF結果顯示，棕色調及黃色調的樣品相較綠色調具有較高比例的錳元素，可以初步判斷棕色調及黃色調的顏色致色成因與錳元素的關聯性。

關鍵字：臺灣閃玉貓眼、閃玉顏色成因、紅外光譜儀、紫外近紅外光譜分析儀、X光螢光分析儀、拉曼光譜儀

Study on Coloration Mechanism of Taiwan Cat's Eye Nephrite

Shih-Yu Wu^{1*}, Chao-Ming Wu^{1,2}, Hung-Yuan Chiang¹

¹Gemifo Co., Taiwan

²Department of Geology, Chinese Culture University

*Corresponding author, E-mail: jennifer.wu@fga-dga-gem.com

Abstract

Research focusing on Taiwan Cat's eye nephrite has been limited. While a variety of research focus on gemological and mineralogical characteristic, currently there is no research focusing on gemological characteristic, the coloration mechanism of Taiwan Cat's eye nephrite.

48 specimens were collected in this research, including various green coloration and yellow or brown coloration. All the specimens were tested under Fourier-transform infrared spectroscopy (FTIR), Ultraviolet Visible Near Infrared Spectroscopy (UV-Visible-NIR), X-ray Fluorescence (XRF) and Raman spectroscopy. The results under UV-Visible-NIR shows that 509nm peak is related to the green coloration and the amount of Fe²⁺; While 509 nm peak is not found in yellowish or brownish specimens. Furthermore, the results from XRF display that higher amount of Mn is found in yellowish and brownish specimens, comparing green specimens. There is a possibility that the yellowish and brownish coloration is related to Mn.

Keywords: Taiwan Nephrite Cat's Eye, Coloration Mechanism of Taiwan Nephrite

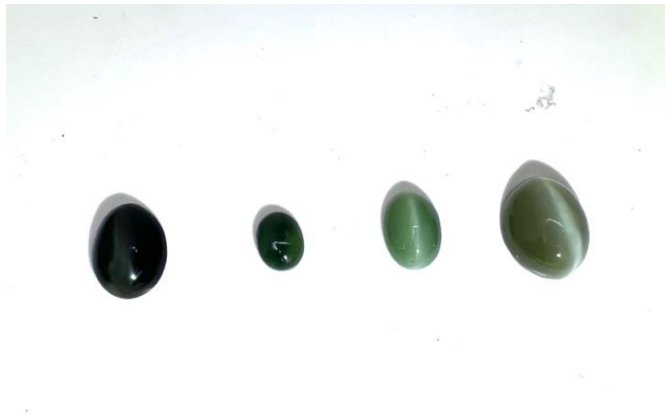


圖1、綠色閃玉的顏色深淺變化。(以4顆樣品為代表)

Fig. 1. Color differences in green nephrites (4 representative nephrites)



圖2、黃色及棕色閃玉樣品。(以2顆樣品為代表)

Fig. 2. Yellow and brown nephrites (2 representative nephrites)

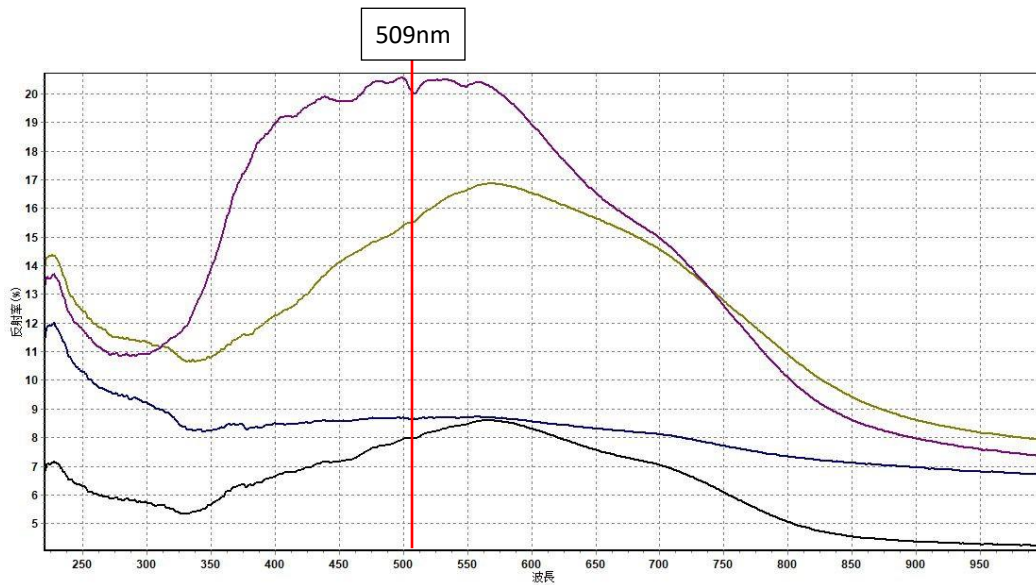


圖3、綠色閃玉樣品在UV-Vis NIR下，可見509nm吸收峰與 Fe^{2+} 有關聯。

(以4顆樣品為代表)

Fig. 3. The results of green nephrites under UV-Vis NIR. 509nm were identified, relating to Fe^{2+} . (4 representative nephrites)

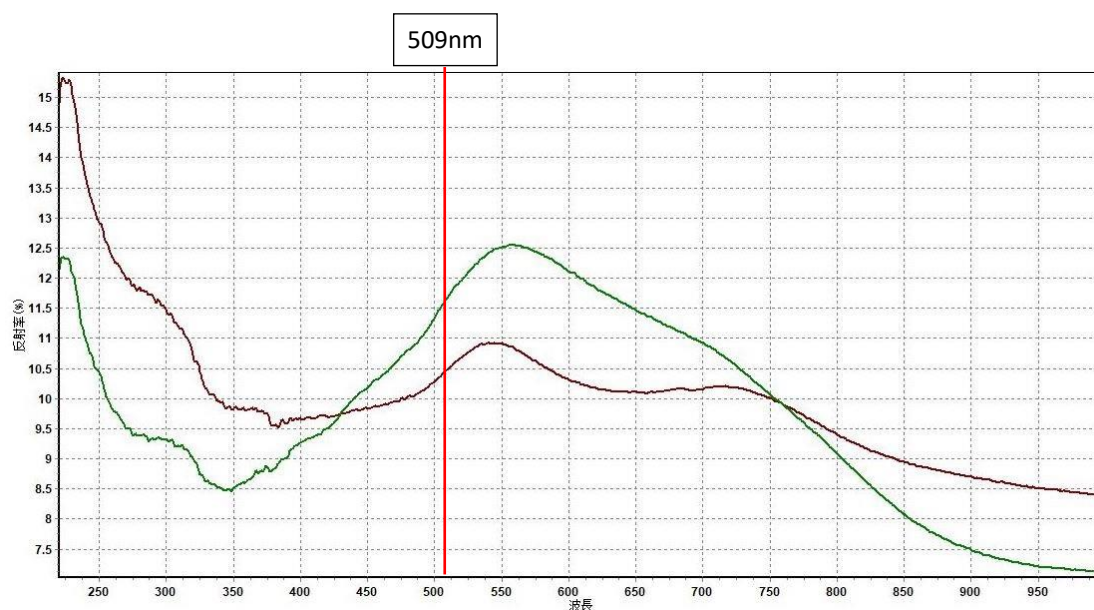


圖4、黃色及棕色樣品在UV-Vis NIR下，未見509nm吸收峰，但有多個吸收峰在350nm-400nm之間，與 Fe^{3+} 有關聯。（以2顆樣品為代表）

Fig. 4. The results of yellow and brown Taiwan nephrites under UV-Vis NIR (2 representative nephrites). 509nm were not identified while several peaks were found between 350nm to 400nm. It is possible related to Fe^{3+} .

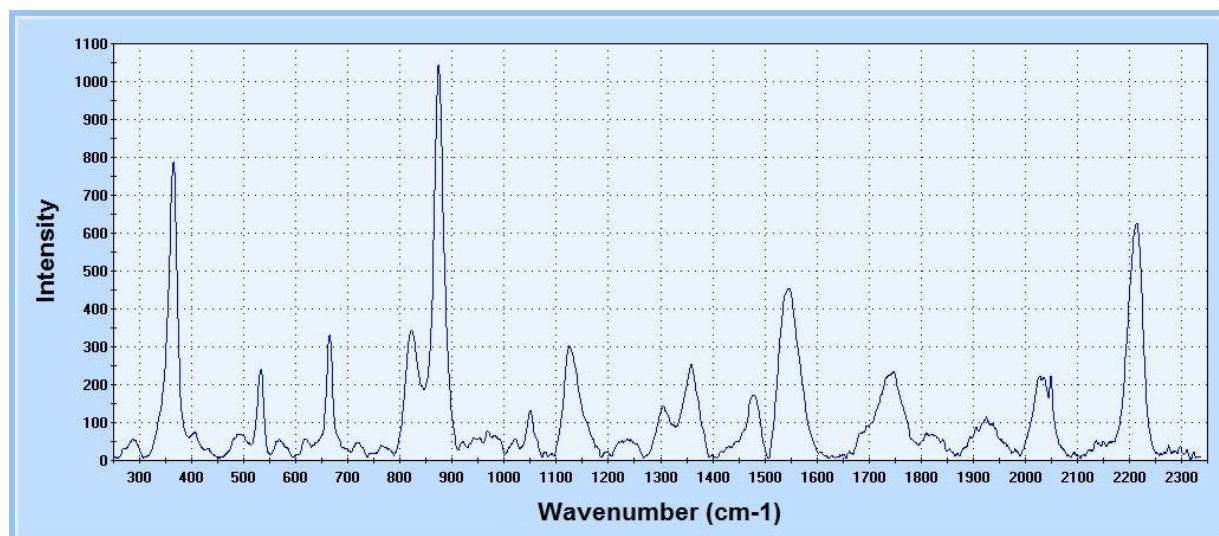


圖5、翠綠色閃玉標本在拉曼光譜的檢測下，偵測到鈣鋁榴石。

Fig. 5. The result of vivid green Taiwan nephrites under Raman spectroscopy. Grossular was found.

臺灣花蓮瑞穗瑞欣礦和壽豐理新礦蛇紋岩中磁鐵礦包裹體的 地球化學研究

Eslam Mohammed Ali Mitwally^{1,2*}、余炳盛¹

¹ 國立臺北科技大學資源工程研究所

² 埃及阿斯烏特愛資哈爾大學科學學院地質系

*通訊作者 E-mail: t107799401@gmail.com

摘要

鎂鐵質和超鎂鐵質岩石因吸水而引起的蝕變過程與蛇紋石化過程有關。在此蛇紋石化過程中，最終成分將是蜥蛇紋石、纖蛇紋石、葉蛇紋石、磁鐵礦(Fe_3O_4)和水鎂石($\text{Mg}(\text{OH})_2$)。當吸附的水在高產條件下氧化鐵橄欖石中的亞鐵(Fe^{2+})離子時，就會形成磁鐵礦。磁鐵礦在其立方尖晶石結構中可以摻入大量微量元素(Fe 、 Al 、 Ti 、 Mg 、 Mn 、 Zn 、 Cr 、 V 、 Ni 、 Co 、 Ga)，它們往往是最實用的指示元素，可能區分磁鐵礦成因。由瑞穗瑞欣礦磁鐵礦顆粒的經驗化學式可以與其他礦區的相互比對。此外，蝕變生成的磁鐵礦的經驗化學式與磁鐵礦顆粒的並不一致，例如其 Co 、 Zn 、 V 和 Ni 較貧化。在壽豐理新礦，磁鐵礦顆粒和蝕變磁鐵礦推導的經驗化學式較為一致，只有 Zn 取代 Al 等少數差異，在蝕變的磁鐵礦經驗化學式中，取代的 Zn 隨著 Al 和 Ti 的富集而被耗盡。PCA 被用於降低數據的複雜性並識別影響礦物成分的元素；並將分析結果與經驗化學得出的結果進行比較。採用實驗式決定從壽豐理新和瑞穗礦獲得的樣品影響磁鐵礦顆粒和蛇紋岩內磁鐵礦斑晶的化學成分中的主要化學元素。這些化學元素是 Fe^{3+} 、 Fe^{2+} 、 Mg 、 Mn 、 Co 、 Cr 和 Si 。影響礦物化學成分的其他化學變量是鋁、鎳、鋅、鈦、鈮和鈣。

關鍵字：蛇紋石、磁鐵礦、主要成分分析、實驗式

Geochemical Study of Magnetite Inclusions in Serpentinite in Ruisui Ruixin and Shoufeng Lixin Mines, in Hualien, Taiwan

Eslam Mohammed Ali Mitwally^{1,2*}, Bing-Sheng Yu¹

¹Institute of Mineral Resources Engineering, National Taipei University of Technology, Taiwan.

²Geology Department, Faculty of Science, Al Azhar University, Assiut, Egypt.

*Corresponding author, E-mail: t107799401@gmail.com

Abstract

The alteration process causing by water adsorb on the mafic and ultramafic rocks leads to serpentinization process. During this serpentinization process, the final components will be Lizardite, chrysotile, magnetite (Fe_3O_4), Brucite ($\text{Mg}(\text{OH})_2$) and antigorite. The magnetite forms when the adsorbed water oxidize ferrous (Fe^{2+}) ions in fayalite in a highly production condition. Magnetite can incorporate a large number of minor and trace elements (Fe, Al, Ti, Mg, Mn, Zn, Cr, V, Ni, Co, and Ga) in its cubic spinel structure, they are often the most practical indicator elements to potentially distinguish magnetite genesis. Empirical formulas derived for the magnetite grains from the Ruisui Ruixin mine were corresponded each other. Also, the empirical formula derived for the altered magnetite was inconsistent with the magnetite grains empirical formulas, such as the depletion of Co, Zn, V, and Ni. On Shoufeng Lixin Mine, the empirical formulas derived for the magnetite grains and altered magnetites were consistent with each other, with only a few differences such as the substitution of Zn instead of Al. The substituted Zn was depleted with the enrichment of Al and Ti in the altered magnetite empirical formula. PCA was used to reduce the complexity of the data and identify elements influencing the compositions of the minerals; the analysis results were compared with those derived using the empirical formulas. The major chemical elements that influenced the chemical compositions of the magnetite grains and patches in the samples obtained from the Shoufeng Lixin and Ruisui mines were determined using empirical formulas. These chemical elements were Fe^{3+} , Fe^{2+} , Mg, Mn, Co, Cr, and Si. Additional chemical variables that influenced the chemical compositions of the minerals were Al, Ni, Zn, Ti, V, and Ca.

Keywords: Serpentine, Magnetite, Principal component Analysis, Empirical formula

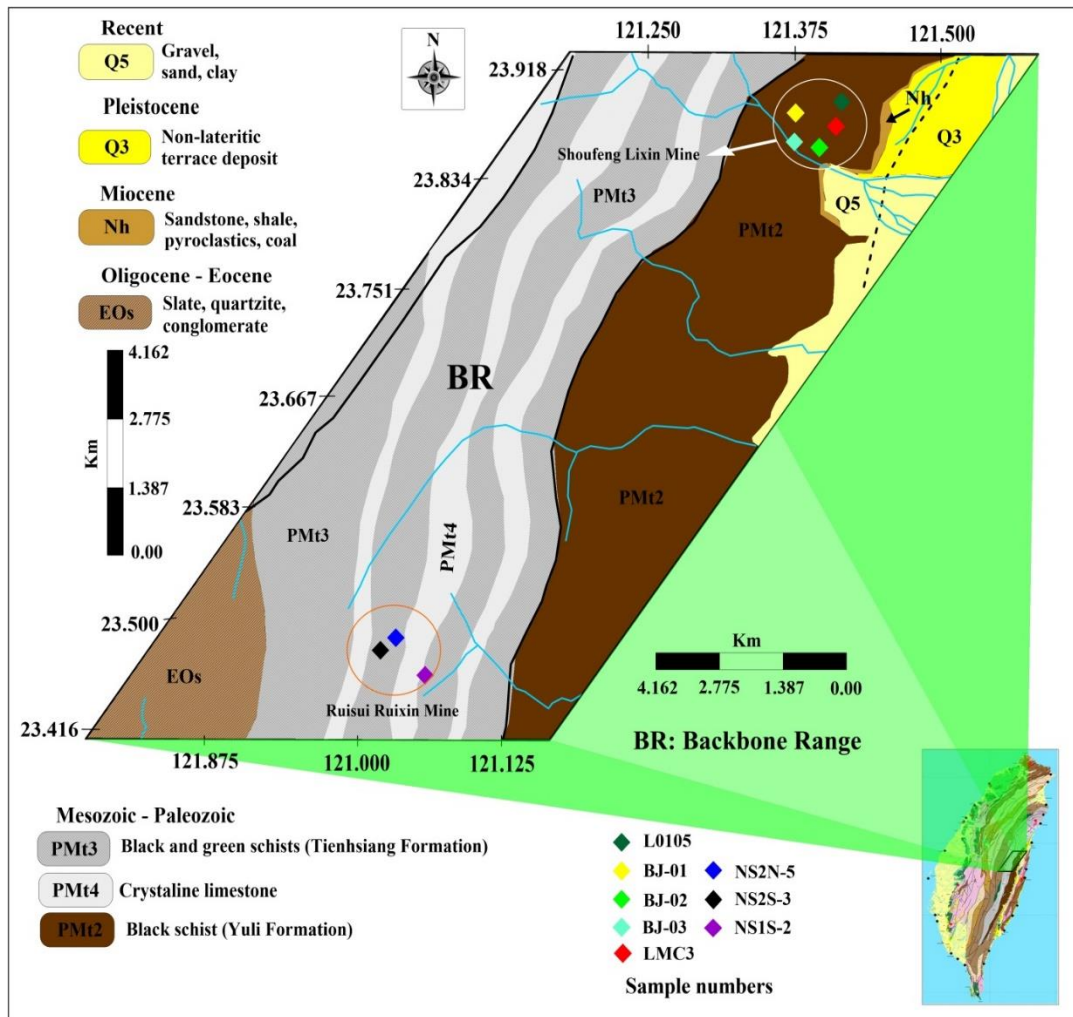


圖1、研究區域的地質和位置圖，蛇紋岩樣品採集自臺灣花蓮的瑞穗瑞欣和壽豐理新兩個礦山。

Fig. 1. Geological and location map of the studied area. Serpentinite samples were collected from two mines, namely Ruisui Ruixin and Shoufeng Lixin mines, in Hualien, Taiwan.

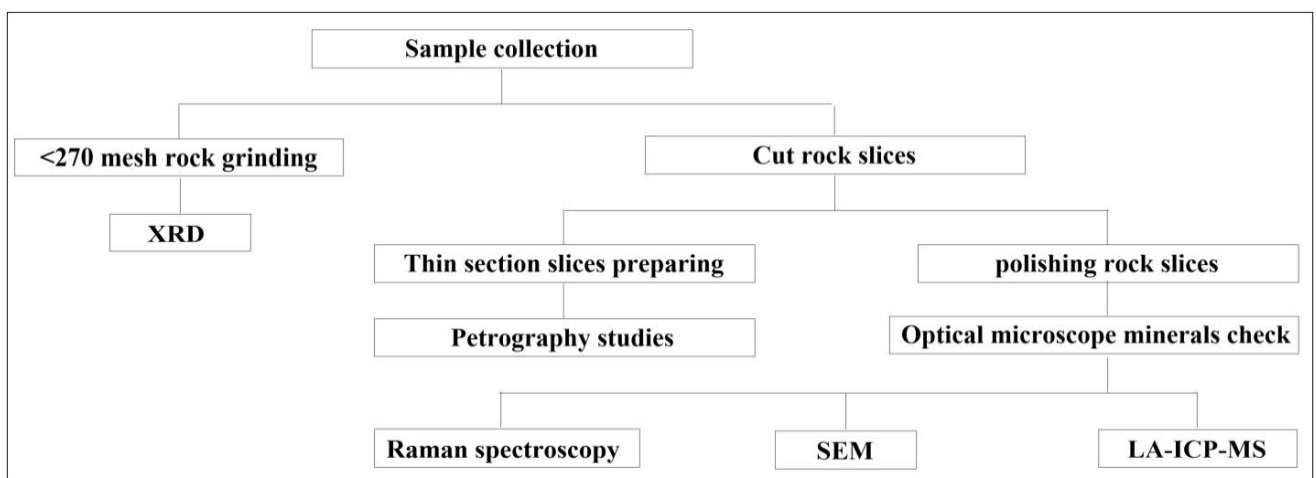


圖2、實驗流程圖和分析方法

Fig. 2. Flowchart of lab operations and analytical methods

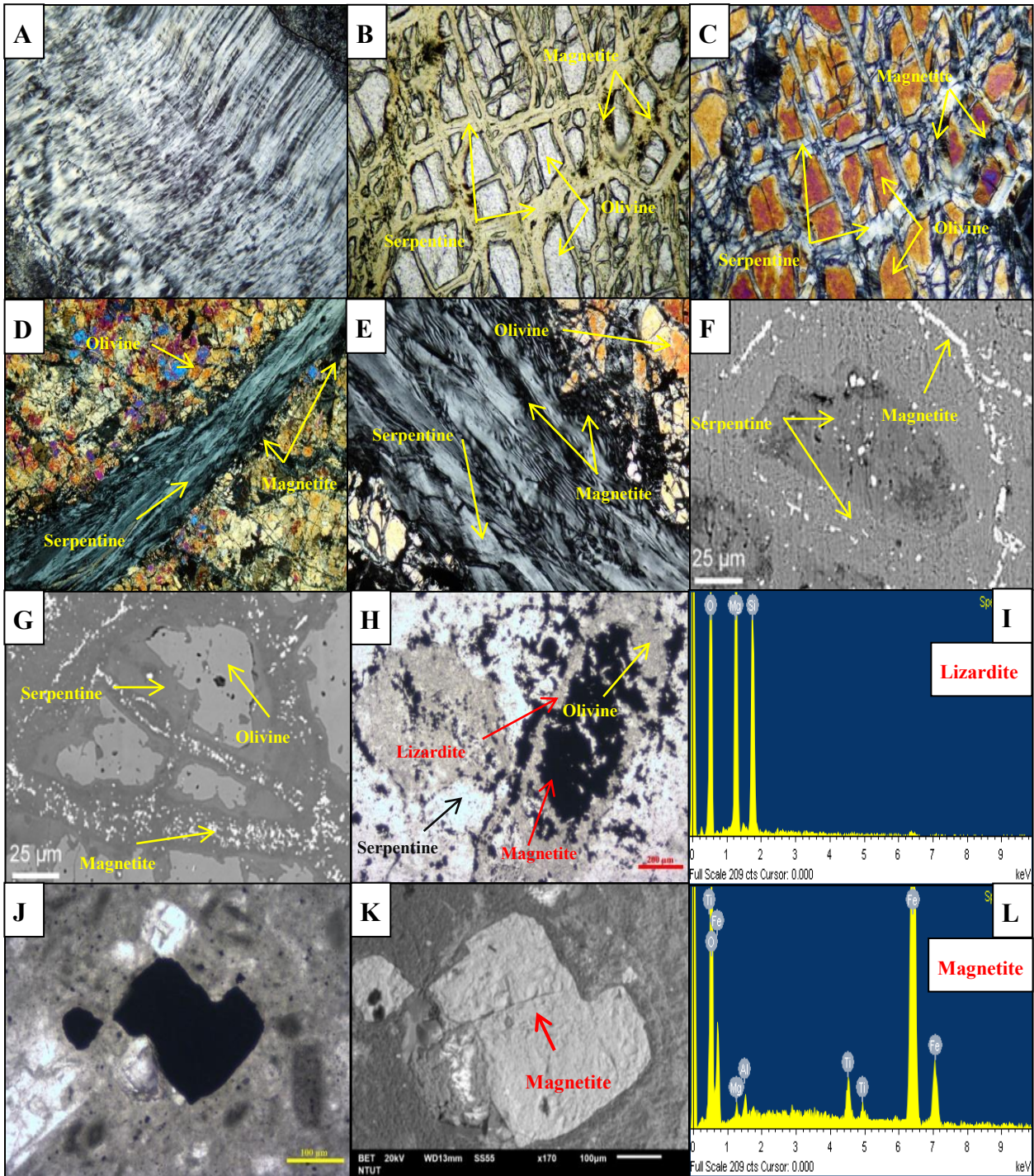


圖 3、[A] 蛇紋石紋理看起來像蛇皮 (XPL 圖像)，[B 和 C] 橄欖石中的網狀結構(高陰影處)，周圍環繞著充滿磁鐵礦的蛇紋石脈(分別為 PPL 和 XPL 圖像)。[D 和 E] 蛇紋石化母岩中的蛇紋石脈 (灰色) (XPL 圖像)。[F] BSE 圖像顯示蛇形網芯和網狀邊緣的完全蛇形網狀紋理，並且可以區分磁鐵礦。[G] BSE 圖像顯示蛇紋石網格邊緣的部分蛇紋石網格紋理，在網格核心中有可見的橄欖石遺跡。[H] 母體橄欖石材料中的主要蛇紋石基質 (PPL 圖像)。[I] 蛇紋石基體的 EDX 結果。[J] 磁鐵礦顆粒 (PPL 圖像)。[K 和 L] 分別是磁鐵礦顆粒的 BSE 圖像和 EDX 結果。

Fig. 3. [A] Serpentine texture look like a snake skin in a serpentinite (XPL image), [B and C] Mesh structure in olivine (high relief) surrounding by serpentine veins filled by magnetite (PPL and XPL images respectively). [D and E] Serpentine vein (grey) in a serpentinized parent rock (XPL images). [F] BSE image showing fully serpentinized mesh texture of serpentine mesh cores and mesh rims, and magnetite can be distinguished. [G] BSE image showing partially serpentinized mesh texture of serpentine mesh rims with visible olivine relicts in the mesh cores. [H] Dominant serpentine groundmass in the parent olivine material (PPL image). [I] EDX result of serpentine ground matrix. [J] Magnetite grain (PPL image). [K and L] BSE images and EDX results of Magnetite grain respectively.

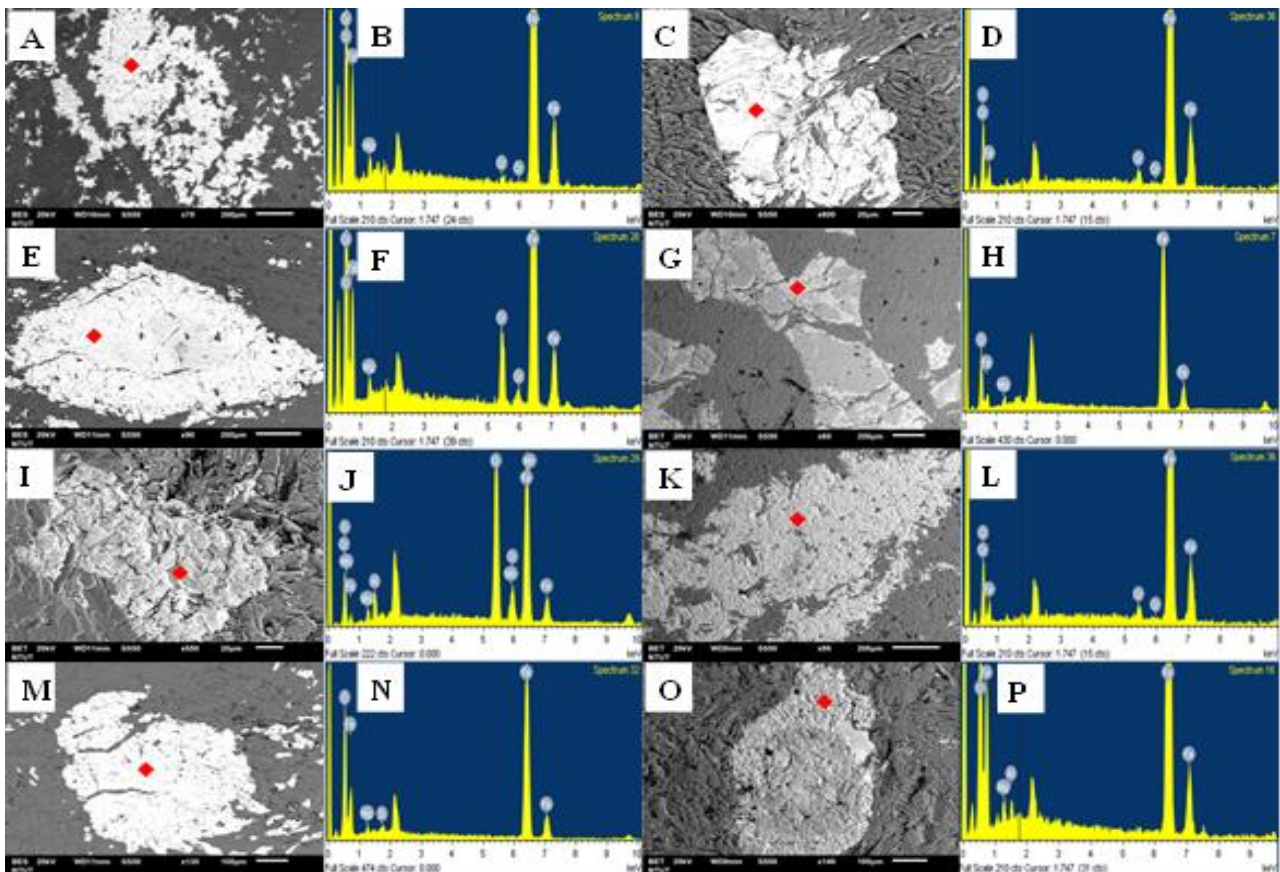


圖 4、研究的蛇紋岩樣品中磁鐵礦的 BES 和 EDX 圖像。除 NS1S-2 和 LMC3 磁鐵礦外，所有研究的磁鐵礦均為具有部分蛇紋岩化的網狀構造，其網的中心為蜥蛇紋石，而邊緣為磁鐵礦（G 和 O）。

Fig. 4. BES and EDX images of the magnetite in the studied serpentinite samples. All the studied magnetite are fully serpentinized mesh texture of magnetite mesh cores and mesh rims, except NS1S-2 and LMC3 magnetite are partially serpentinized mesh texture of lizardite mesh cores and magnetite mesh rims (G and O).

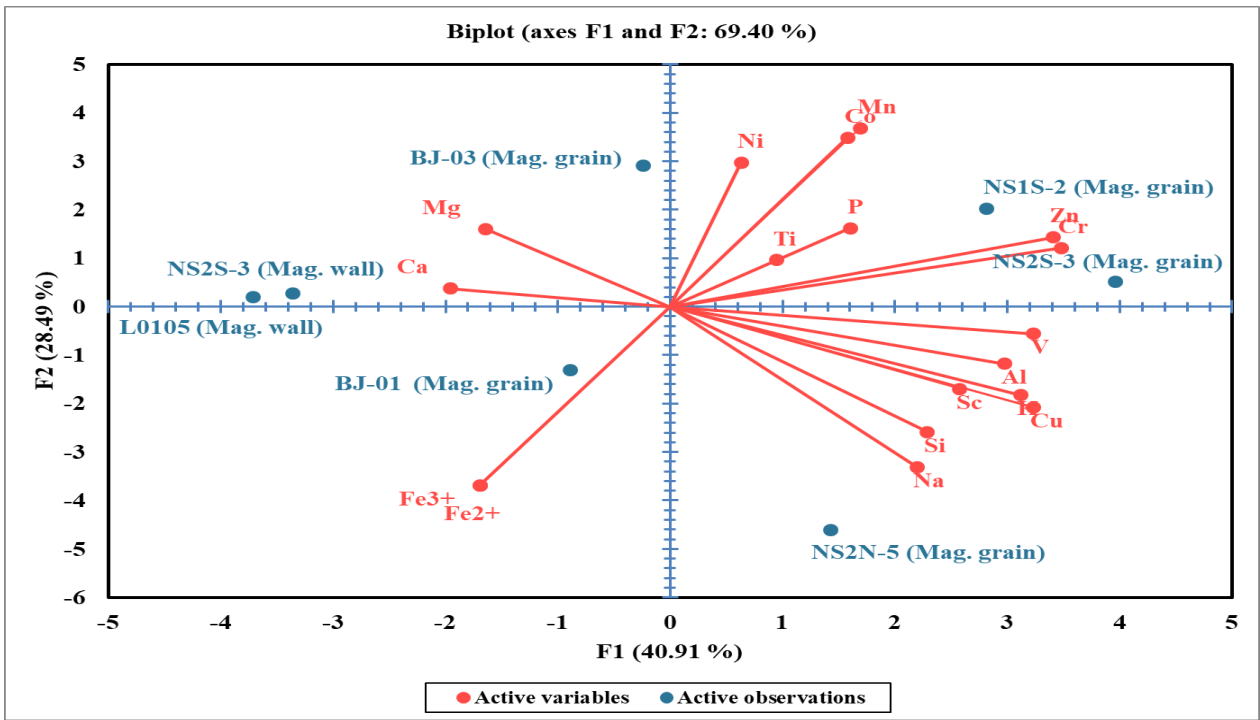


圖5、主成分分析 (PCA) 雙標圖顯示兩個函數 (F1 = 40.91% 和 F2 = 28.49%) 與化學元素 (變量) 和研究樣本 (目標) 的最高可變性之間的關係。

Fig. 5. Principal component analysis (PCA) biplot indicating the relationship between the two functions (F1 = 40.91% and F2 = 28.49%) with the highest variability of the chemical elements (variables) and studied samples (objectives).

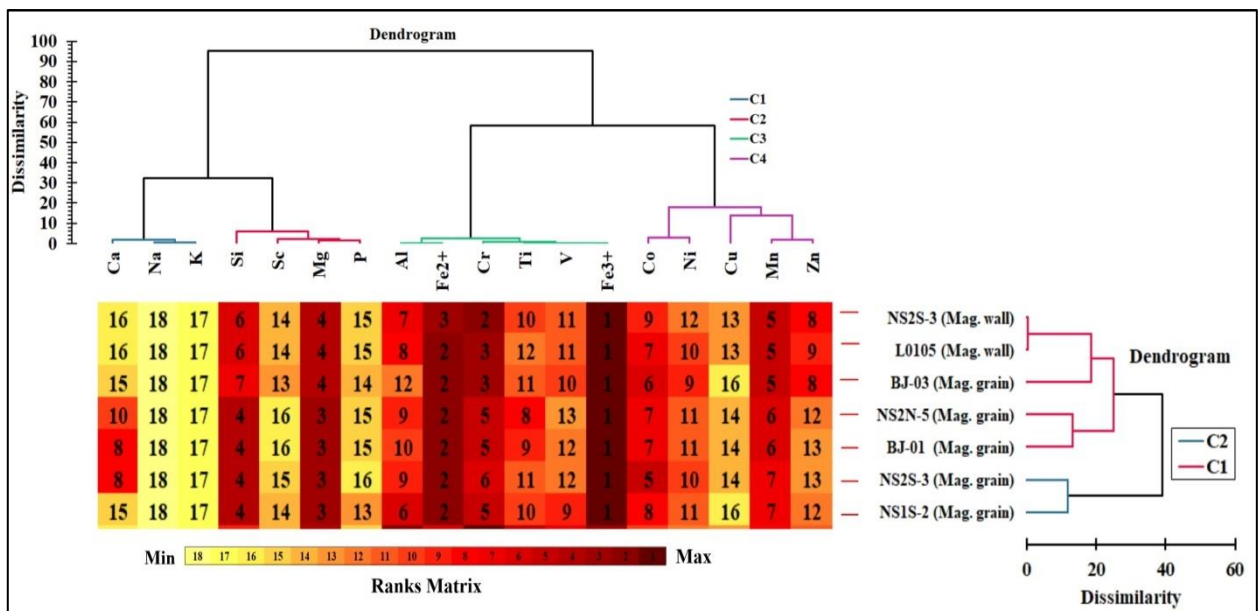


圖6、用於確定影響磁鐵礦樣品化學成分的主要化學元素的層次聚類 (A和B) 和排序模型 (C) 結果。分層垂直聚類 (A) 揭示了四個主要聚類 (C1 - C4)，其中C1包括Ca、Na和K；C2包括Si、Sc、Mg和P；C3包括Al、Fe²⁺、Cr、Ti、V和Fe³⁺；C4包括Co、Ni、Ca、Mn和Zn。層次水平聚類 (B) 揭示了兩個主要集群

(C1和C2)，其中C1包括NS2S-3 (Mag.grain) 和NS1S-2 (Mag.grain)；C2包括BJ-03 (Mag.grain)、NS2S-3 (Mag.wall)、L0105 (Mag.wall)、BJ-01 (Mag.grain) 和NS2N-5 (Mag.grain)。

Fig. 6. Hierarchical clustering (A and B) and ranking model (C) results for determining major chemical elements influencing the chemical compositions of magnetite samples. Hierarchical vertical clustering (A) revealed four major clusters (C1-C4), where C1 included Ca, Na, and K; C2 included Si, Sc, Mg, and P; C3 included Al, Fe²⁺, Cr, Ti, V, and Fe³⁺; and C4 included Co, Ni, Ca, Mn, and Zn. Hierarchical horizontal clustering (B) revealed two major clusters (C1 and C2), where C1 included NS2S-3 (Mag. grain) and NS1S-2 (Mag. grain); and C2 included BJ-03 (Mag. grain), NS2S-3 (Mag. wall), L0105 (Mag. wall), BJ-01 (Mag. grain), and NS2N-5 (Mag. grain).

表 1、研究樣本採集位置

Table 1. Sample collection locations in study area

| Sa. no. | Latitude | Longitude | remarks | Location |
|---------------|---------------|-----------------|--------------|------------------------------|
| BJ-01 | 23°51'14.0" N | 121° 25'57.1" E | Serpentinite | Shoufeng Lixin Mine, Hualian |
| BJ-02 | 23°50'26.78"N | 121°26'39.48"E | Serpentinite | Shoufeng Lixin Mine, Hualian |
| BJ-03 | 23°40'13.55"N | 121°24'15.22"E | Serpentinite | Shoufeng Lixin Mine, Hualian |
| NS1S-2 | 23°29'21.6"N | 121°18'12.8"E | Serpentinite | Ruisui Mine, Hualian |
| NS2S-3 | 23°29'22.37"N | 121°18'10.5"E | Serpentinite | Ruisui Mine, Hualian |
| NS2N-5 | 23°29'25.43"N | 121°18'10.8"E | Serpentinite | Ruisui Mine, Hualian |
| L0105 | 23°51'39.63"N | 121°27'9.68"E | Serpentinite | Shoufeng Lixin Mine, Hualian |
| LMC3 | 23°50'57.29"N | 121°27'3.08"E | Serpentinite | Shoufeng Lixin Mine, Hualian |

表 2、本研究的蛇紋岩樣品中磁鐵礦的經驗公式

Table 2. Empirical formulas of the magnetite in the studied serpentinite samples

| Sa. no. | Empirical formula |
|---------------|---|
| NS2S-3 | (Fe ²⁺ _{0.303} Mg _{0.039} Mn _{0.028} Co _{0.006} Zn _{0.007} Ni _{0.001})(Fe ³⁺ _{0.908} Cr _{0.310} Al _{0.012} Si _{0.023} Ti _{0.002} V _{0.001}) ₂ O _{4.640} |
| NS1S-2 | (Fe ²⁺ _{0.294} Mg _{0.172} Mn _{0.055} Co _{0.010} Zn _{0.007} Ni _{0.001})(Fe ³⁺ _{0.881} Cr _{0.240} Si _{0.026} Al _{0.008} Ti _{0.001} V _{0.001}) ₂ O _{4.086} |
| NS2N-5 | (Fe ²⁺ _{0.409} Mg _{0.050} Mn _{0.003} Co _{0.002})(Fe ³⁺ _{1.227} Cr _{0.009} Al _{0.005} Si _{0.042} Ti _{0.001} V _{0.001}) ₂ O _{4.676} |
| NS2S-3 | (Fe ²⁺ _{0.346} Mg _{0.121} Mn _{0.005} Co _{0.003} Ca _{0.001})(Fe ³⁺ _{1.037} Cr _{0.005} Si _{0.008} Al _{0.001} Ti _{0.001}) ₂ O _{3.733} |
| BJ-01 | (Fe ²⁺ _{0.403} Mg _{0.077} Mn _{0.003} Co _{0.013} Ca _{0.003} Ni _{0.001})(Fe ³⁺ _{1.208} Cr _{0.008} Al _{0.002} Si _{0.038}) ₂ O _{4.526} |
| BJ-03 | (Fe ²⁺ _{0.335} Mg _{0.075} Mn _{0.021} Co _{0.020} Zn _{0.002} Ni _{0.002})(Fe ³⁺ _{1.004} Cr _{0.156} Si _{0.010}) ₂ O _{4.451} |
| L0105 | (Fe ²⁺ _{0.351} Mg _{0.143} Mn _{0.004} Co _{0.004} Ca _{0.001} Ni _{0.001})(Fe ³⁺ _{1.054} Cr _{0.006} Si _{0.007} Al _{0.001} Ti _{0.001}) ₂ O _{3.773} |

表 3、礦物化學成分中含量較高的主要元素的相關係數。

Table 3. Correlation coefficient of the basic elements chemical elements with relatively high concentrations in the chemical compositions of minerals.

| BCE | Fe ³⁺ | Fe ²⁺ |
|------------------|------------------|------------------|
| Na | -0.103 | -0.094 |
| Mg | 0.450 | 0.441 |
| Al | 0.238 | 0.265 |
| Si | 0.838 | 0.865 |
| P | -0.692 | -0.674 |
| K | -0.497 | -0.479 |
| Ca | 0.453 | 0.400 |
| Sc | -0.432 | -0.424 |
| Ti | 0.859 | 0.832 |
| V | 0.862 | 0.844 |
| Cr | 0.588 | 0.562 |
| Mn | 0.185 | 0.159 |
| Fe ³⁺ | 1 | 0.974 |
| Fe ²⁺ | 0.974 | 1 |
| Co | 0.582 | 0.529 |
| Ni | 0.247 | 0.229 |
| Cu | -0.221 | -0.238 |
| Zn | 0.571 | 0.553 |

BCE = Basic Correlation Element

表 4、觀測值的平方餘弦

Table 4. Squared cosines of observations

| | F1 | F2 | F3 | F4 | F5 |
|--------|-------|-------|-------|-------|-------|
| BJ-01 | 0.001 | 0.566 | 0.005 | 0.117 | 0.005 |
| BJ-03 | 0.212 | 0.458 | 0.008 | 0.258 | 0.001 |
| NS1S-2 | 0.287 | 0.052 | 0.175 | 0.359 | 0.007 |
| NS2N-5 | 0.033 | 0.038 | 0.085 | 0.087 | 0.699 |
| NS2S-3 | 0.324 | 0.022 | 0.560 | 0.009 | 0.003 |
| L0105 | 0.031 | 0.565 | 0.292 | 0.080 | 0.004 |
| NS2S-3 | 0.036 | 0.562 | 0.230 | 0.042 | 0.000 |

表 5、變量的平方餘弦

Table 5. Squared cosines of variables

| | F1 | F2 | F3 | F4 | F5 |
|------------------------|-----------|-----------|-----------|-----------|-----------|
| Na | 0.000 | 0.173 | 0.446 | 0.210 | 0.014 |
| Mg | 0.446 | 0.270 | 0.038 | 0.002 | 0.192 |
| Al | 0.003 | 0.841 | 0.000 | 0.011 | 0.085 |
| Si | 0.760 | 0.012 | 0.084 | 0.025 | 0.060 |
| P | 0.568 | 0.060 | 0.004 | 0.184 | 0.009 |
| K | 0.303 | 0.015 | 0.499 | 0.077 | 0.024 |
| Ca | 0.195 | 0.281 | 0.013 | 0.210 | 0.163 |
| Sc | 0.421 | 0.511 | 0.002 | 0.002 | 0.033 |
| Ti | 0.849 | 0.057 | 0.005 | 0.015 | 0.013 |
| V | 0.853 | 0.117 | 0.000 | 0.000 | 0.003 |
| Cr | 0.454 | 0.342 | 0.000 | 0.146 | 0.009 |
| Mn | 0.372 | 0.123 | 0.175 | 0.061 | 0.141 |
| Fe³⁺ | 0.727 | 0.053 | 0.058 | 0.098 | 0.012 |
| Fe²⁺ | 0.693 | 0.056 | 0.063 | 0.125 | 0.010 |
| Co | 0.739 | 0.060 | 0.063 | 0.045 | 0.022 |
| Ni | 0.293 | 0.410 | 0.081 | 0.004 | 0.025 |
| Cu | 0.079 | 0.405 | 0.245 | 0.016 | 0.134 |
| Zn | 0.783 | 0.002 | 0.150 | 0.045 | 0.005 |

表 6、影響研究樣本化學組成的化學元素（按層次垂直聚類排序）。

Table 6. Chemical elements (sorted in hierarchical vertical clustering) influencing chemical compositions of study samples.

| | C1 | C2 | C3 | C4 |
|---------------|-----------|-----------|---|----------------|
| BJ-01 | Ca | Mg, Si | Cr, Fe ³⁺ , Fe ²⁺ , Al | Mn, Co, Ni |
| BJ-03 | | Mg, Si | Cr, Fe ³⁺ , Fe ²⁺ | Mn, Co, Ni, Zn |
| NS1S-2 | | Mg, Si | Cr, Fe ³⁺ , Fe ²⁺ , Al, Ti, V | Mn, Co, Ni, Zn |
| NS2N-5 | | Mg, Si | Cr, Fe ³⁺ , Fe ²⁺ , Al, Ti, V | Mn, Co |
| NS2S-3 | | Mg, Si | Cr, Fe ³⁺ , Fe ²⁺ , Al, Ti, V | Mn, Co, Ni, Zn |
| L0105 | Ca | Mg, Si | Cr, Fe ³⁺ , Fe ²⁺ , Al, Ti | Mn, Co, Ni |
| NS2S-3 | Ca | Mg, Si | Cr, Fe ³⁺ , Fe ²⁺ , Al, Ti | Mn, Co |

C1, 2, 3, and 4= Clustering 1, 2, 3, and 4

表 7、研究區蛇紋岩中磁鐵礦經驗公式計算和 PCA 技術檢測出的影響化學元素的排列。

Table 7. Arrangement of the influential chemical elements which detected from the empirical formula calculation and PCA technique of magnetite in serpentinite rocks at the study area.

| | | Fe ³⁺ | Fe ²⁺ | Mg | Cr | Si | Mn | Co | Al | Ni | V | Ti | Zn | Ca |
|---------------|---------------|------------------|------------------|-----|-----|-----|-----|------|------|------|------|------|------|------|
| NS2S-3 | Em. F. | 1st | 2nd | 4th | 3rd | 6th | 5th | 11th | 8th | 13th | 13th | 12th | 9th | - |
| | Ranking model | 1st | 3rd | 4th | 2nd | 6th | 5th | 9th | 7th | 12th | 11th | 10th | 8th | 16th |
| BJ-03 | Em. F. | 1st | 2nd | 4th | 3rd | 7th | 5th | 6th | - | 8th | - | - | 8th | - |
| | Ranking model | 1st | 2nd | 4th | 3rd | 7th | 5th | 6th | 12th | 9th | 10th | 11th | 8th | 15th |
| NS2S-3 | Em. F. | 1st | 2nd | 3rd | 5th | 4th | 5th | - | 6th | - | - | 6th | - | 6th |
| | Ranking model | 1st | 2nd | 3rd | 5th | 4th | 6th | 7th | 9th | 11th | 13th | 8th | 12th | 10th |
| L0105 | Em. F. | 1st | 2nd | 3rd | 5th | 4th | 6th | 6th | 7th | 7th | - | 7th | - | 7th |
| | Ranking model | 1st | 2nd | 3rd | 5th | 4th | 6th | 7th | 10th | 11th | 12th | 9th | 13th | 8th |
| BJ-01 | Em. F. | 1st | 2nd | 3rd | 6th | 4th | 7th | 5th | 8th | 8th | - | - | - | 7th |
| | Ranking model | 1st | 2nd | 3rd | 6th | 4th | 7th | 5th | 9th | 10th | 12th | 11th | 13th | 8th |
| NS2N-5 | Em. F. | 1st | 2nd | 3rd | 5th | 4th | 7th | 8th | 6th | - | 9th | 9th | - | - |
| | Ranking model | 2nd | 2nd | 3rd | 5th | 4th | 7th | 8th | 6th | 11th | 9th | 10th | 12th | 15th |

拉利瑪海紋石的祕密

陳惠芬^{1*}、黃浩珉²、史羽弘³

¹ 國立臺灣海洋大學地球科學研究所

² 中國文化大學地質研究所

³ 多明尼加琥珀寶石鑑定所

*通訊作者 E-mail: diopside0412@yahoo.com.tw

摘要

有著海水般波浪紋路的藍綠色半寶石 Larimar，其類似矽孔雀石藍玉髓的顏色十分令人著迷。過去都認為這種藍綠色調的成因應該是銅離子所造成，今日我們將為您揭開顏色與波浪紋路的祕密。Larimar 是由放射針狀的針鈉鈣石所形成的集合體，與一般針鈉鈣石不同之處在於其特殊的藍綠色調。發現者 Migu Eslam Méndezm 以女兒的名字“Larissa”結合西班牙語的海洋“mar”命名為“Larimar”。雖然針鈉鈣石在全世界產地很多，但目前有這種藍綠色調的針鈉鈣石僅產於多明尼加 Baoruco 地區。為何在全球這麼多個針鈉鈣石的產地之中，只有多明尼加的 Baoruco 地區能產出這種藍綠色針鈉鈣石？

研究結果顯示 pectolite 與 calcite、natrolite 或少量的自然銅顆粒充填於嚴重風化的玄武岩孔洞或裂隙內，該處的玄武岩多已風化或經過紅土化作用。由地質研究的文獻指出此地區的玄武岩確實有較高濃度的鈳。而比較過藍色、綠色、白色 pectolite 中的鐵、銅、鈳、鈦、鈷等可能造成藍色或綠色成因的微量元素後，推測導致 pectolite 呈現藍色的主要因為鈳離子，而造成綠色的原因主要為鐵離子，並非過去所認為的銅離子致色。自然銅的沉澱基本上主要發生於溶液充填孔洞的初期，因為銅離子溶解於強酸性溶液，當流體轉變為弱鹼性條件才會沉澱出 pectolite 與 calcite。此時的狀態下銅離子早已沉澱為顆粒狀的自然銅，因此與 pectolite 結晶分離。另外，其放射針狀晶體的結構亦造成顏色上的差異，促使放射中心點顏色較深，而邊緣的顏色較淺。邊緣的纖維晶體排列混亂造成光的漫反射效應則產生了波浪紋路。這種現象猶如纖維狀平行排列的礦物造成的貓眼效應類似，都是纖維排列所造成的。

關鍵字：多明尼加、針鈉鈣石、玄武岩、纖維狀、鈳、鐵

The Secret of Wave-like Larimar

Huei-Fen Chen^{1*}、Hao-Ming Huang²、Yu-Hong Shih³

¹Institute of Earth Sciences, National Taiwan Ocean University

²Institute of Earth Sciences (Geology Program), Chinese Culture University

³Laboratorio Dominicano de Ámbar y Gemas, Santo Domingo 10149, República Dominicana

*Corresponding author, E-mail: diopside0412@yahoo.com.tw

Abstract

Larimar, a blue-green semi-precious stone with a wave-like pattern and color similar to chrysocolla-chalcedony, is fascinating. It was previously believed that the cause of this blue-green hue was due to the trace element of copper. Today, we will uncover the secret behind the color and wave patterns. Larimar is a collective formed by radiating needle-shaped crystals of pectolite. It owns unique blue-green hue in different with common pectolites. The discoverer, Miguel Méndez, named the stone "Larimar" by combining his daughter's name "Larissa" with the Spanish word for ocean "mar". Although needle-shaped pectolite is found in many locations worldwide, the blue-green variety is currently only found in the Baoruco region of the Dominican Republic. Why is the blue-green pectolite only produced in the Baoruco region of the Dominican Republic in so many pectolites from other locations around the world?

The research results indicate that pectolite grows with calcite, natrolite, or small amounts of natural copper particles, fills the severely weathered cavities or fractures in basalt. The basalt in this location has mostly undergone weathering or laterization. Geological literature indicates that the basalt in this region does indeed have higher concentrations of vanadium. After comparing the trace elements such as iron, copper, vanadium, titanium, and cobalt in blue, green, and white pectolite, which may cause the blue or green coloration, it is suggested that the primary reason for blue coloration in pectolite is vanadium ions, while the main reason for green coloration is iron ions, not copper ions as previously thought. The precipitation of natural copper mainly

occurs in the early stage of solution-filled cavities, as copper ions dissolve in strongly acidic solutions and precipitate as pectolite and calcite only when the fluid changes to weak alkaline conditions. In precipitation processes, the copper ions have already precipitated as granular natural copper and are separated from pectolite crystallization. In addition, the structure of its radiating needle-shaped crystals also causes differences in color, with the color being darker at the center of the radiation point and lighter at the edges. The disordered arrangement of fibrous crystals at the edges causes a diffuse reflection of light, producing a wave-like pattern. This phenomenon is similar to the cat's eye effect caused by minerals with parallel fiber-like arrangements, both of which are caused by fiber alignment.

Keywords: Dominican, pectolite, basalt, fibrous, vanadium, iron

表 1、全球針鈉鈣石分布地（表格原始資料來自 Mindat 資料網站）。

Table 1. Global distributions of pectolites (The data was cited from the web of Mindat)

| 產地 | |
|-----|---------------------------|
| 亞洲 | 日本、印度 |
| 歐洲 | 義大利、俄羅斯、德國 |
| 美洲 | 美國（紐澤西州、內華達州、阿肯色州、加州）、格陵蘭 |
| | 拉丁美洲：多明尼加、巴西、阿根廷 |
| 非洲 | 坦桑尼亞、馬達加斯加 |
| 大洋洲 | 澳大利亞、紐西蘭 |

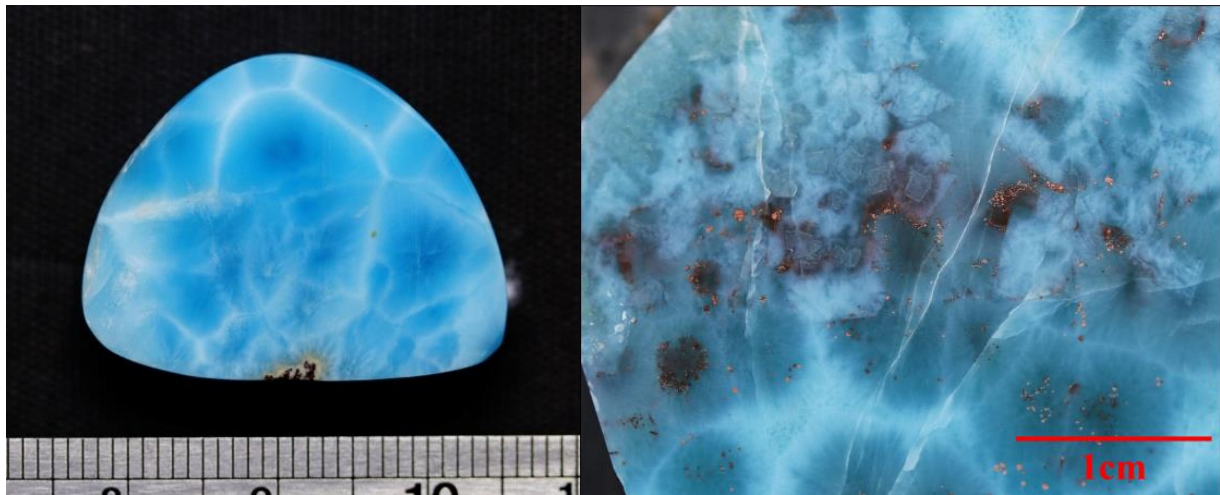


圖 1、水藍色波紋的寶石級藍色針鈉鈣石，這類針鈉鈣石中經常可以看縫隙中
充填有自然銅晶體。

Fig. 1. Cyan pectolite with wave-like pattern has gem quality, and there is often native copper in the interstitial filling of pectolites.

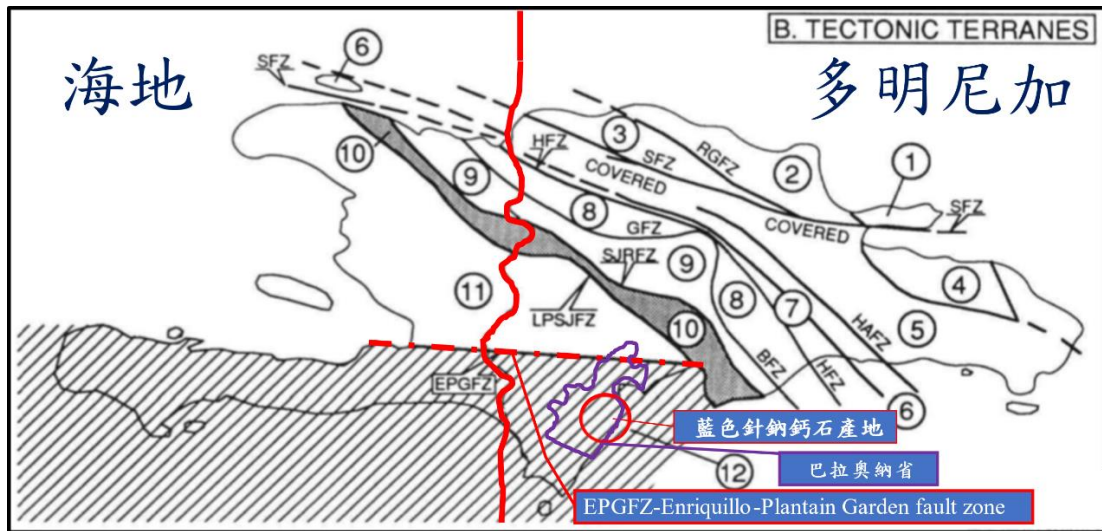


圖 2、伊斯帕尼奧拉島（又稱西班牙島）之地質構造帶劃分，斜線處之紅圈區域極為藍色針鈉鈣石產區（原圖摘自 Mann et al., 1991）。

Fig. 2. The tectonic divisions of Hispaniola Island. The red circle means the original place of cyan pectolite (The figure was cited from Mann et al., 1991).

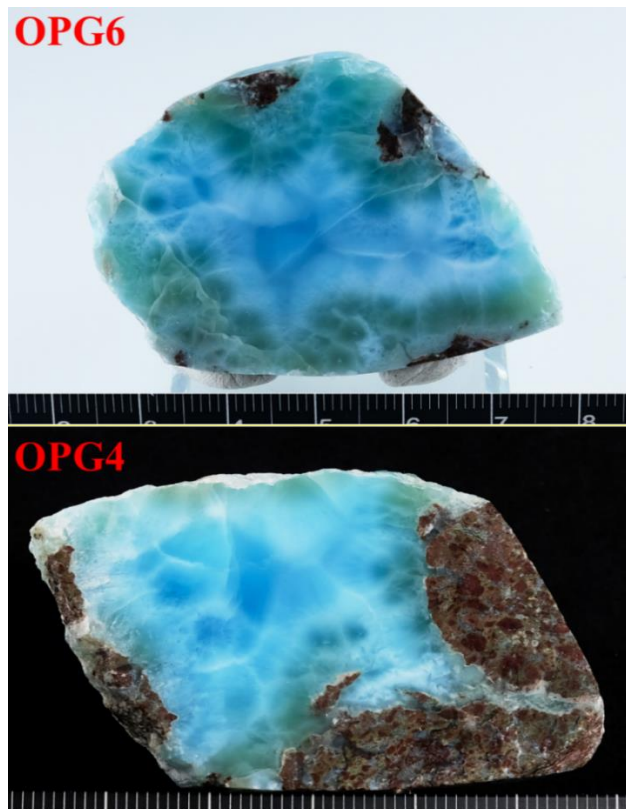


圖 3、針鈉鈣石的綠色部分幾乎靠著圍岩分布，中心則較接近藍色，而周圍風化的紅色玄武岩富含赤鐵礦。

Fig. 3. The green pectolite almost distributes along the wall rocks, which are altered basalt rich in hematite, and the blue pectolite concentrates in the center.

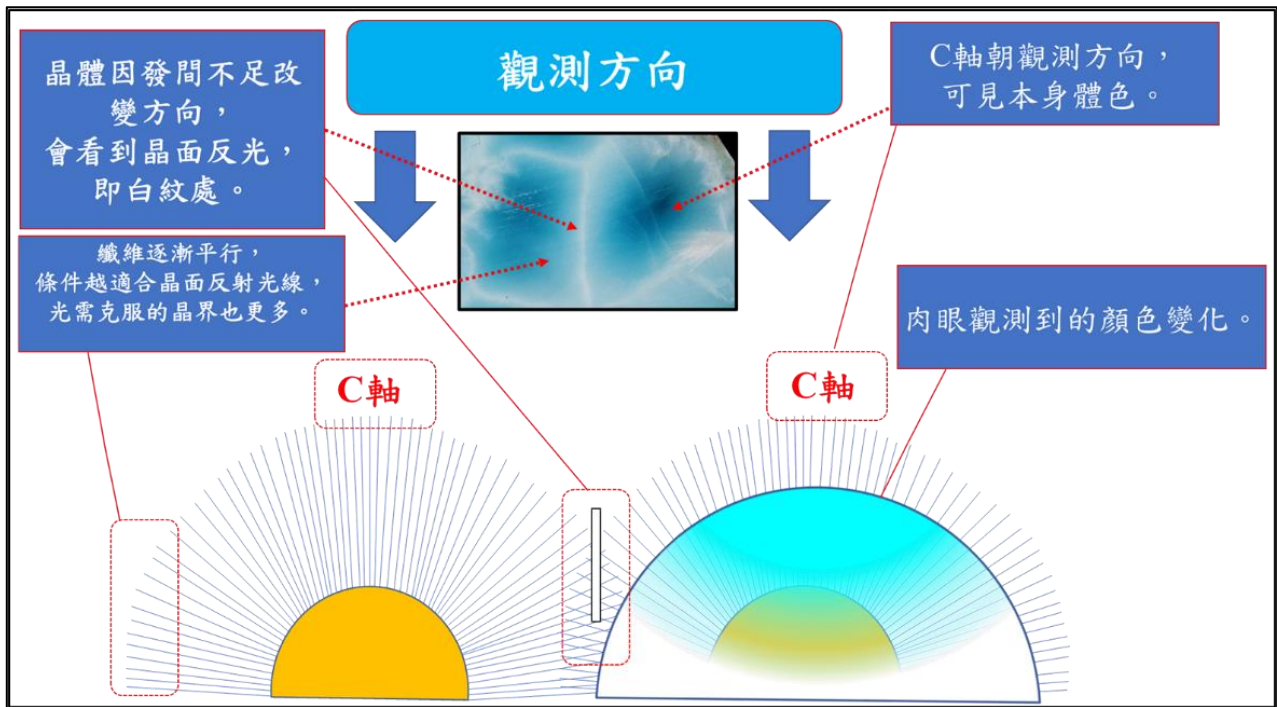


圖 4、放射球狀的藍色針鈉鈣石結構造成觀測者因為結晶排列方向的改變，導致觀測到的顏色在靠近中心處較深，靠近放射球邊緣的顏色反白。

Fig. 4. The texture of radial and spherical blue pectolite causes the observed color to be darker near the center, and the color near the edge of the radial sphere is white due to the change of the crystal direction of the observer.

寶石包裹體之評估模式與應用

陳淑娟

義守大學工業管理學系

E-mail : melinda2085@yahoo.com.tw

摘要

寶石包裹體的重要性對於寶石鑑定專家與珠寶業者來說，是區分天然寶石、合成寶石、優化處理寶石與品質分級等的關鍵指標。受過專業訓練的珠寶鑑定專家或珠寶經營者對於寶石的包裹體大多能根據經驗與學習的程度作出正確判斷。然而對於目前許多當舖業者、新創業者或年輕電商來說，如何能夠運用較有效率的資源與簡易的方法來學習與認識寶石包裹體，是目前常見與需要解決的問題。

因此本研究運用層級分析法的概念，以天然剛玉、合成剛玉包裹體與仿品為例，將液體、氣體、固體包裹體等與合成寶石的特徵包裹體系統性的整理分析與比較。再以資料包絡分析法中的 CCR 模式，根據寶石業者對於寶石的淨度、顏色與切工之不同的需求，建立選擇最佳化的寶石的方法，提供寶石業者較為合理的選擇依據。本研究之目的希望能將寶石學專家對於包裹體之認知，以較為系統性與邏輯性的觀念，給予新的學習者一個較簡易與正確的學習方法。

關鍵字：寶石包裹體、天然剛玉、層級分析法、CCR 模式

The Evaluation Model and Application of Gemstone Inclusions

Shu-Chuan Chen

Department of Industrial Management, I-SHOU University, Taiwan (R.O.C.)

E-mail: melinda2085@yahoo.com.tw

Abstract

The importance of gemstone inclusions is a key indicator for gem identification professionals and jewelry to distinguish natural gemstones, synthetic gemstones, treated gemstones, and the quality grading of gemstones. Most professionally trained experts or jewelry operators can make the right judgment about gemstone inclusions based on their experience and learning. However, for many pawnshops, new entrepreneurs or young e-commerce companies, how to use more efficient resources and simple methods to learn and understand gemstone inclusions is a common problem that needs to be solved.

Therefore, this study uses the concept of Analytic Hierarchy Process(AHP), taking natural corundum, synthetic corundum inclusions and imitations as examples, moreover systematically analyzes and compares liquid, gas, solid inclusions, etc. with the characteristic inclusions of synthetic gemstones.

Then use the CCR model in the data envelopment analysis method to establish a method for selecting the best gemstones according to the gemstone industry's different needs for the clarity, color and cut of gemstones, and provide the gemstone industry with a reasonable basis for selection. The purpose of this research is to provide new learners with a simpler and more accurate learning method by giving gemologists a systematic and logical understanding of inclusions.

Keywords: gemstone inclusions, natural corundum, Analytic Hierarchy Process, CCR model



圖 1、合成紅寶石弧形生長紋

Fig. 1. Curved lines in synthetic ruby

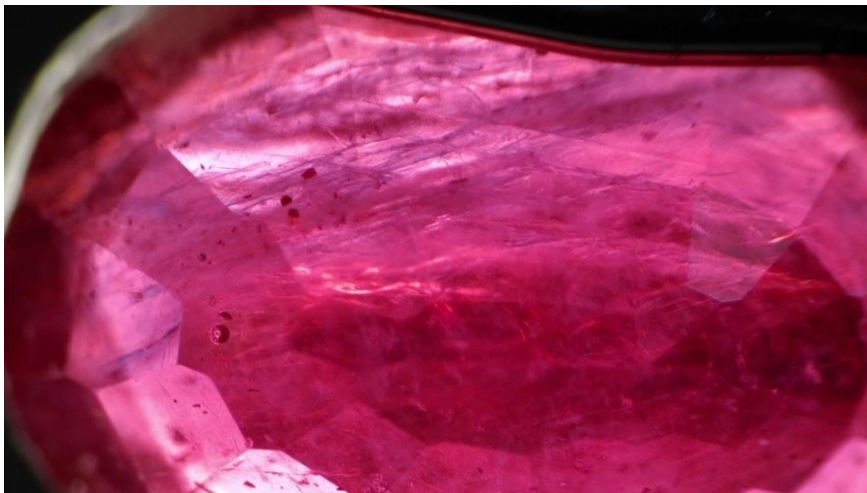


圖 2、玻璃充填紅寶石的氣泡與藍色閃光

Fig. 2. Flash effect and bubbles in lead glass filled ruby

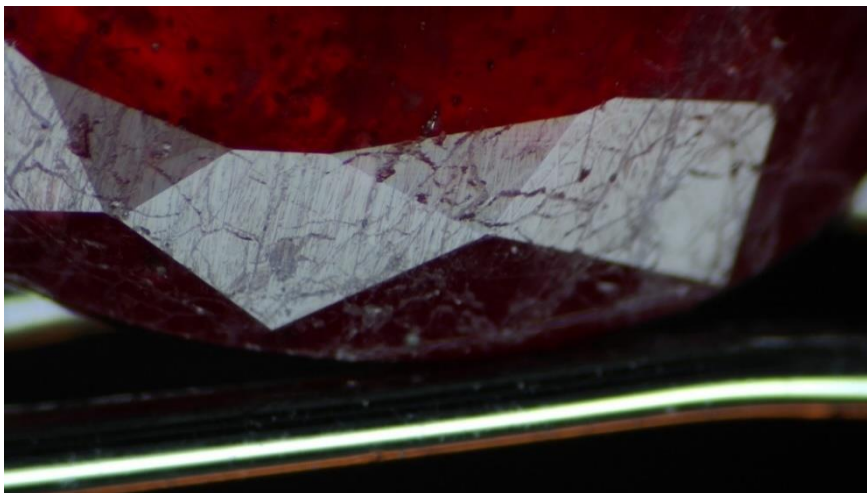


圖 3、頂光照明：玻璃充填紅寶石表面裂隙

Fig. 3. Bright field illumination: surface-reaching fractures in glass filled ruby

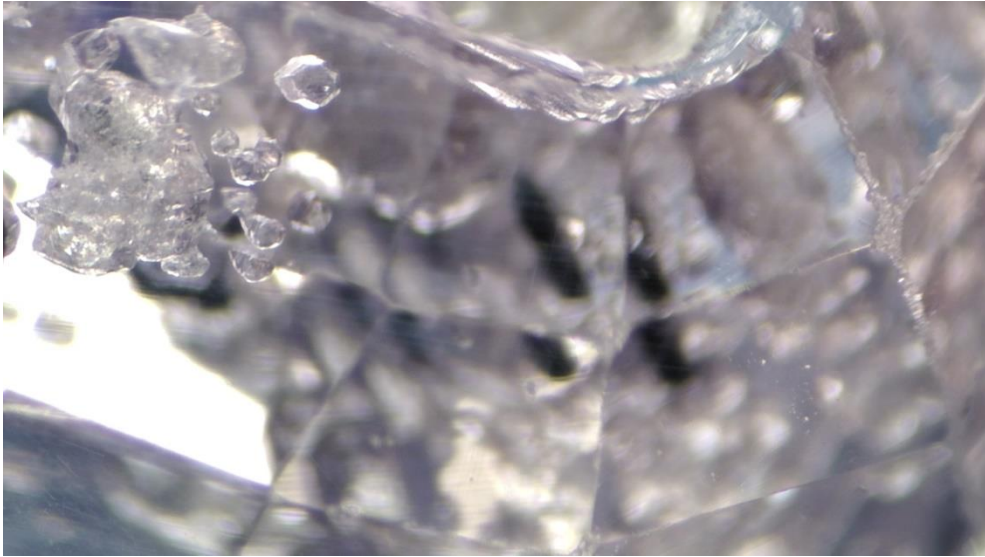


圖 4、剛玉固體包裹體

Fig. 4. Solid inclusions in Corundum



圖 5、Poly Chrome 4K Pro CCD 顯微鏡 (3840x2160)

Fig. 5. Poly Chrome 4K Pro CCD Microscope (3840x2160) microscope

多變量統計在寶石學上的應用-以玻隕石和黑曜岩鑑定為例

林書弘^{1,2*}、潘惠娟³、陳惠芬¹

¹ 國立臺灣海洋大學地球科學研究所

² 臺灣聯合珠寶玉石鑑定中心

³ 國立臺灣海洋大學海洋工程科技中心

*通訊作者 E-mail: slin@tulab.com.tw

摘要

寶石學中所謂的天然玻璃泛指天然產出的富二氧化矽非晶質固體，其成因大致可區分為火山源與非火山源成因兩類，前者包括黑曜岩及玄武岩玻璃，後者則有玻隕石、焦石英、假玄武岩玻璃或閃電熔岩等。在野外，部分玻隕石與黑曜岩因為外觀和成分相似所以時常相互混淆，甚至常規寶石學測試也難以區分之，而且兩者在價格上有所差異，因此造成交易市場之亂象。因此，本研究希望透過 X 光螢光分析結合多變量統計方法，嘗試區分黑曜岩與玻隕石等天然玻璃的差異與產地來源。

本研究分析了來自美洲、亞洲與澳洲等產地共 326 件天然玻璃樣本，包括已知玻隕石與黑曜岩樣本，以及來自美國亞利桑那州、哥倫比亞和印尼等三產地的未分類天然玻璃樣本。所有樣本先經由顯微觀察與顯微拉曼光譜儀分析其包體以驗證分類是否正確，再使用能量散射式 X 光螢光光譜儀 (Bruker S1-Titan 800 EDXRF) 做為半定量分析工具，於標樣校正後分析各產地之天然玻璃成分。縱然 X 光螢光光譜儀僅為半定量工具，卻是珠寶業內較常見且相對容易取得的非破壞性分析儀器。本研究的檢測樣本皆為天然玻璃，成分相對均勻，採用 X 光螢光光譜儀將天然玻璃種類進行鑑定及產地來源分類時，藉由大面積的分析區域達到平均的效果(3mm 準直器，X 光覆蓋 3mm 直徑的圓)，相較於顯微 EDXRF 或 SEM-EDS 更適用於本研究。

為了解析不同種類的天然玻璃與多種元素間的關係，本研究採用主成分分析 (PCA) 對自變數 (元素成分含量除以鉀含量之比值) 降維，提取能區分天然玻璃種類或產地的最佳自變數組合作為新的主成分。接著再用提取的主成分荷重組合與自變數做迴歸分析，以瞭解主成分與元素成分之間的關係式，進而建立分類模型，並評估分類模型的可行性。

研究結果發現，主成分分析與迴歸分析等多變量統計方法配合 EDXRF 分析確實可有效區分捷克玻隕石、澳亞群玻隕石與黑曜岩，甚至進一步區分部分黑曜岩與玻隕石之產地來源。

關鍵字：黑曜岩、捷克玻隕石、澳亞群玻隕石、主成分分析、迴歸分析

Multivariate Statistics Application in Gemology

- Using The Identification of Tektites and Obsidian as Examples

Shu-Hong Lin^{1,2*}, Hui-Juan Pan³, Huei-Fen Chen¹

¹Institute of Earth Sciences, National Taiwan Ocean University, Keelung, Taiwan

²TULAB of Gem Research, Inc., Taipei, Taiwan

³Center of Excellence for Ocean Engineering

*Corresponding author, E-mail: slin@tulab.com.tw

Abstract

In gemology, natural glass refers to silica-rich amorphous solid which is naturally produced of either volcanic or non-volcanic origin. The former includes obsidian and basaltic glass, while the latter includes tektites, lechatelierite, pseudotachylyte and fulgurite. In the field, some tektites and obsidians are often confused with each other because of their similar appearance and composition, making it difficult to distinguish them even with regular gemological tests. As a result, there is often chaos in the trading market due to the price difference between these tektites and obsidians. This study aims to use EDXRF analysis combined with multivariate statistical methods to differentiate natural glasses such as obsidian and tektite and further determine their sources.

This research analyzed a total of 326 natural glass samples from various sources, including known tektite and obsidian samples from America, Asia, and Australia, as well as unclassified natural glass samples from three sources: Arizona, Colombia, and Indonesia. All samples were first examined with microscope and micro-Raman analysis to confirm their varieties. EDXRF (Bruker S1-Titan 800 EDXRF) was further used to analyze the composition of natural glasses from various sources after standards calibration. Although X-ray fluorescence spectrometry is only a semi-quantitative tool, it is a common and relatively easy-to-obtain non-destructive analytical instrument in the jewelry industry. The samples analyzed in this study were all natural glasses with

relatively homogeneous compositions. When using X-ray fluorescence spectrometry to classify natural glasses and identify their origins, the use of a large scanning area helps to achieve average effects (3 mm collimator, X-ray coverage of a 3 mm diameter circle), which is more suitable for this research than micro-EDXRF or SEM-EDS.

In order to analyze the relationship between different types of natural glasses and their composition, principal component analysis (PCA) was used to reduce the dimension of the independent variables (the ratio of element content to potassium content) and to extract the best combination of independent variables that can distinguish the types or sources of natural glasses as new principal components. Finally, the extracted principal component loadings and independent variables were adopted for regression analysis to find out the relationship between the principal components and compositions. In this way, it would be possible to establish classification models and evaluate their feasibility.

It is found that the combination of multivariate statistical methods such as PCA and regression analysis with EDXRF analysis can effectively distinguish moldavite, Australasian tektite, and obsidian; besides, the geographic origins of some obsidians and tektites can also be determined with this method.

Keywords: Obsidian, Moldavite, Australasian tektites, PCA, Regression

表 1、本研究中所採用的天然玻璃類校正組與驗證組樣本之數據列表。(修改自林書弘，2023。天然玻隕石和黑曜岩之地球化學與統計方法鑑定，國立臺灣海洋大學地球科學所博士論文，31 頁)

Table 1. The data list of the natural glass samples used in this study, including calibration set and verification set. (Modified from Lin, S.H., 2023. Identification of Natural Tektite and Obsidian by Geochemical and Statistical Methods, Ph.D. thesis, Institute of Earth Sciences, NTOU, pp.31)

| 樣本代碼 | 樣本類型 | 產地來源 | 校正組 數據筆數 | 驗證組 數據筆數 |
|---------|---------|-----------|-------------|-------------|
| NG-CO | 未分類天然玻璃 | 哥倫比亞 | 19 | 5 |
| NG-AZ | 未分類天然玻璃 | 美國亞利桑那州 | 25 | 5 |
| NG-ID | 未分類天然玻璃 | 印尼 | 25 | 5 |
| OBS-APA | 黑曜岩 | 美國亞利桑那州 | 17 | 5 |
| OBS-CA | 黑曜岩 | 美國北加州戴維斯溪 | 30 | 5 |
| OBS-JP | 黑曜岩 | 日本北海道上藻別 | 10 | 5 |
| OBS-MX | 黑曜岩 | 墨西哥 | 20 | 5 |
| TEK-CZ | 濺射型玻隕石 | 捷克 | 25 | 5 |
| TEK-TH | 濺射型玻隕石 | 泰國 | 38 | 5 |
| TEK-VN | 濺射型玻隕石 | 越南 | 25 | 5 |
| TEK-PH | 濺射型玻隕石 | 菲律賓 | 19 | 5 |
| TEK-AU | 濺射型玻隕石 | 澳洲 | 13 | 5 |

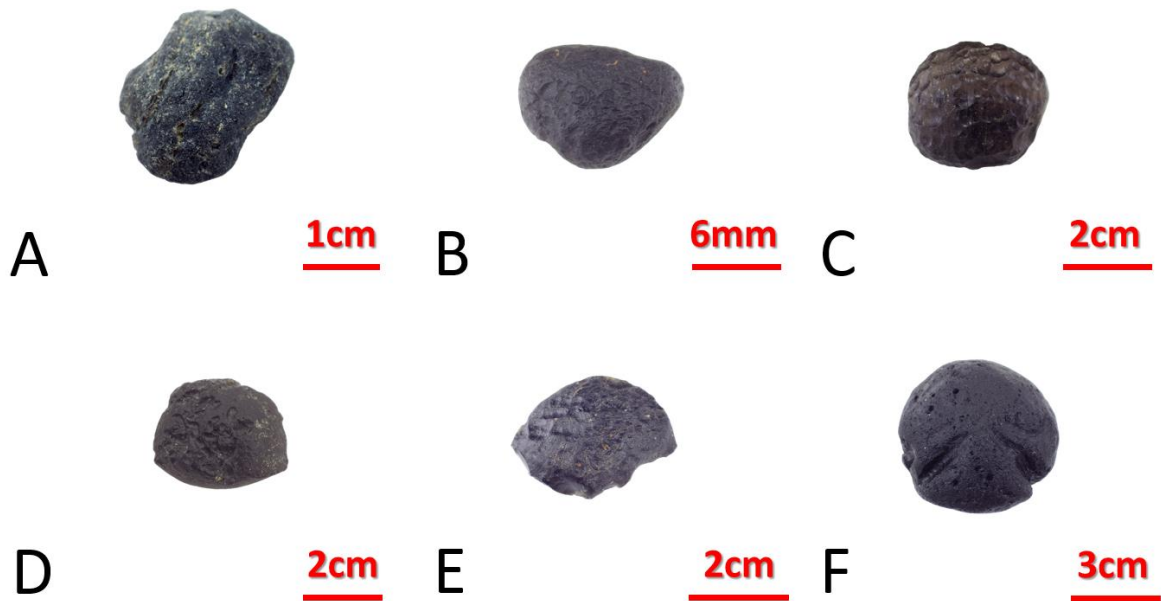


圖 1、市場上來自不同產地以玻隕石名義銷售的天然玻璃：(A)來自印尼、(B)來自美國亞利桑那、(C)來自哥倫比亞、(D)來自泰國、(E)來自越南，以及(F)來自菲律賓，在後續的驗證中確認 A、B、C 三者為黑曜岩，而 D、E、F 三者則是已知為澳亞群玻隕石。

Fig. 1. Natural glasses sold under the name of tektite from different origins in the market: (A) from Indonesia, (B) from Arizona in the United States, (C) from Colombia, (D) from Thailand, (E) from Vietnam, and (F) from the Philippines. In subsequent verification, it was confirmed that A, B, and C are obsidian, while D, E, and F are known to be Australasian tektite.



圖 2、圖左為能量散射式 X 光螢光光譜儀 (Bruker S1-Titan 800 EDXRF)，其規格為：3mm 準直器，電壓 50kV，電流 200 μ A Max，矽漂移偵測器 (FASTTM SDD)，解析度 $<145\text{eV}$ ，可分析鎂 Mg(12)~鈾 U(92)。圖右可見樣本放置平台及其量測的面積示意圖。

Fig. 2. The left is an energy dispersive X-ray fluorescence spectrometer (Bruker S1-Titan 800 EDXRF), which features a 3 mm collimator, 50 kV voltage, 200 μ A max current, and a silicon drift detector (FASTTM SDD) with a resolution of $<145\text{ eV}$. It is capable of analyzing elements from magnesium (Mg-12) to uranium (U-92). On the right is the sample placement platform and a schematic diagram of the measurement area.

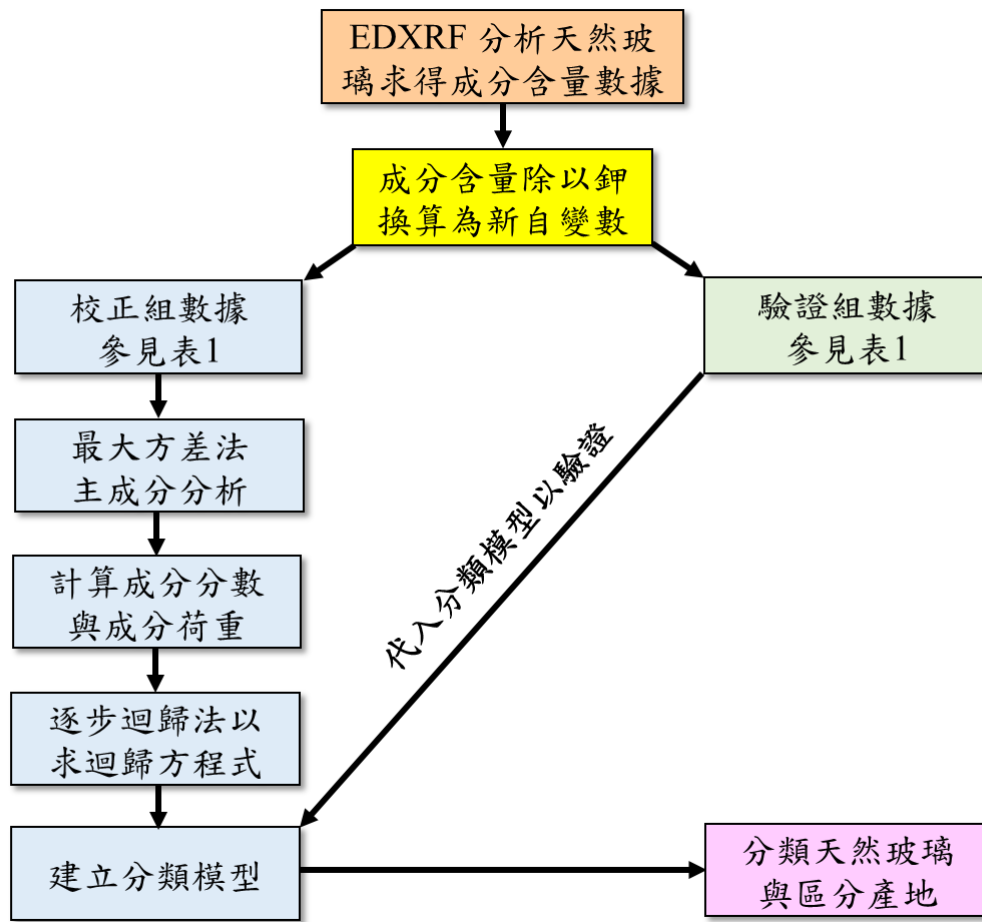


圖 3、本研究所採用之多變量統計方法相關研究流程圖（修改自林書弘，2023。天然玻璃隕石和黑曜岩之地球化學與統計方法鑑定，國立臺灣海洋大學地球科學所博士論文，32 頁）。

Fig. 3. Flowchart for Multivariate Statistical Methods adopted in this Research. (Modified from Lin, S.H., 2023. Identification of Natural Tektite and Obsidian by Geochemical and Statistical Methods, Ph.D. thesis, Institute of Earth Sciences, NTOU, pp.32)

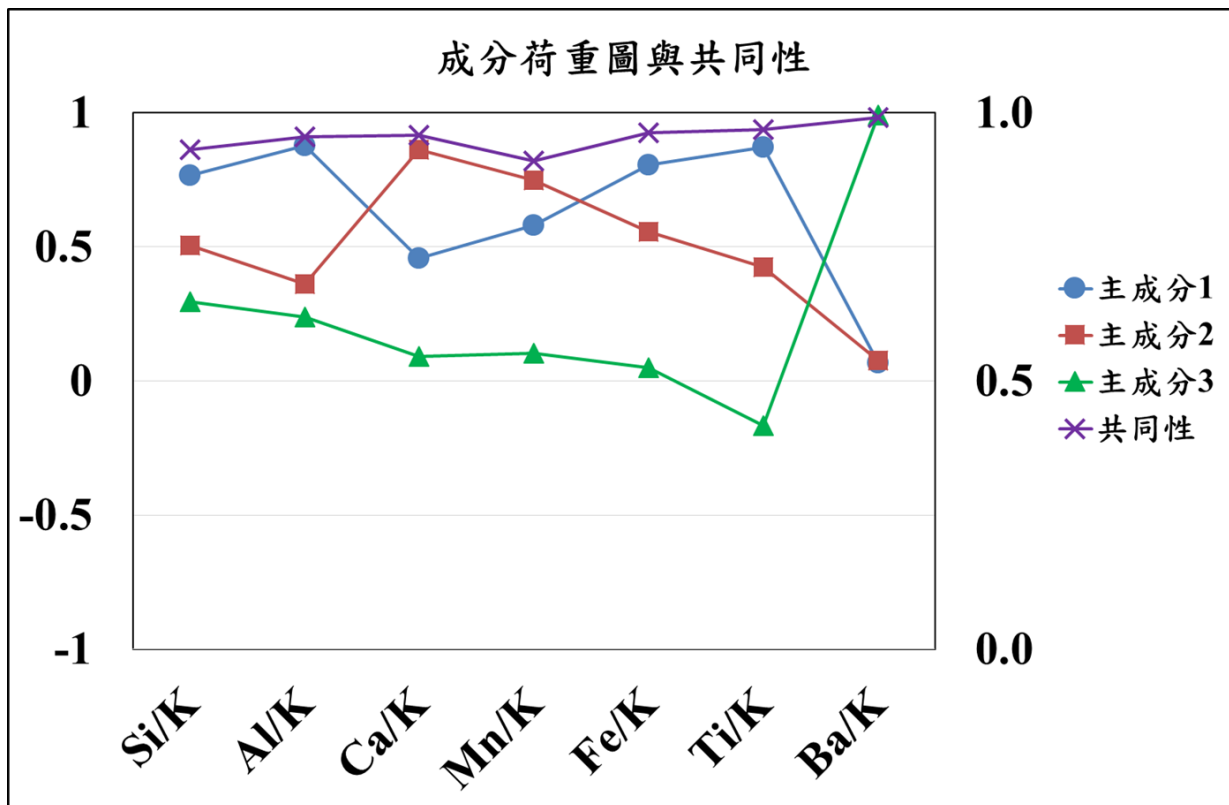


圖 4、本模型的成分荷重圖與共同性，圖中可見三個主成份與七個自變數的相關性（左側主軸）以及各自變數的提取參數共同性高低（右側副軸）。

Fig. 4. The component loading and communality of this model are shown in the graph. On the left main axis, the correlations between three main components and seven independent variables can be seen. On the right secondary axis, the extraction parameters of each independent variable and their communality are displayed.

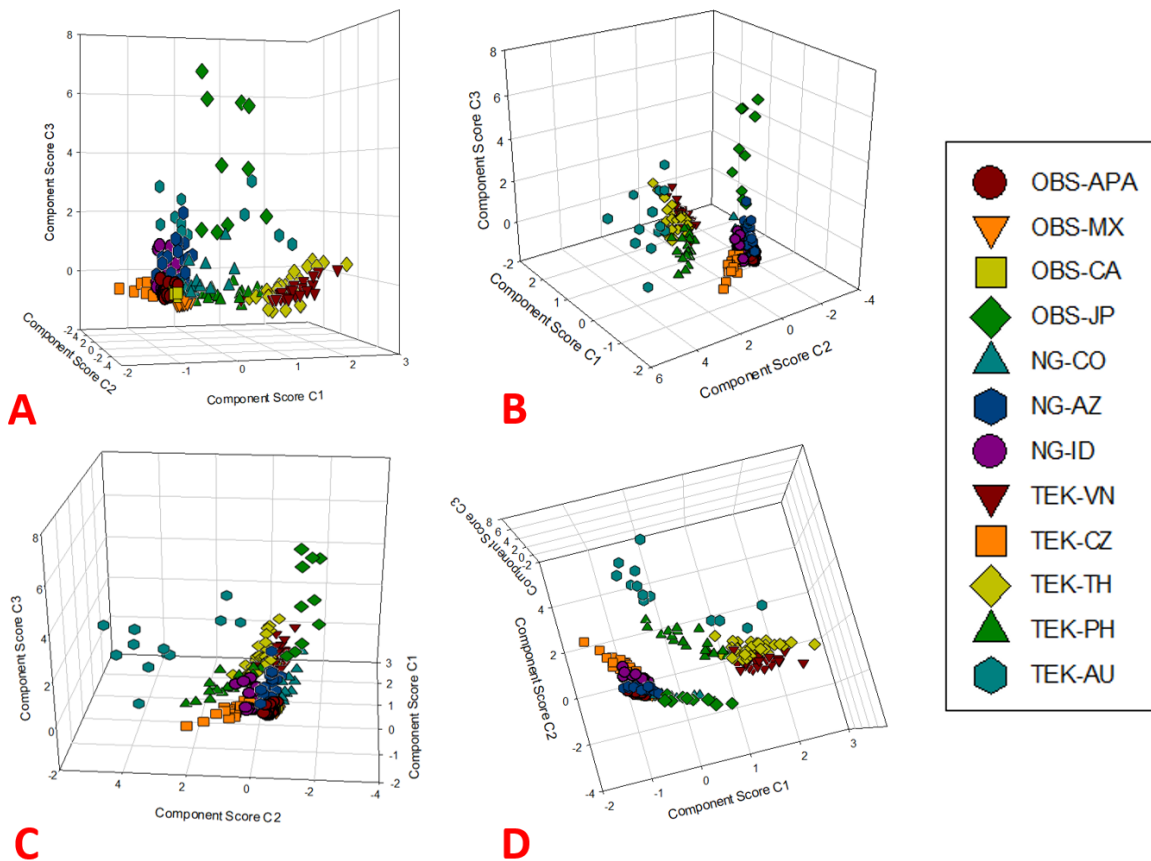


圖 5、天然玻璃分類模型校正組數據之成分分數 3 維散佈圖，A-D 為同一個圖形旋轉不同角度，如此可以更清楚觀察出不同產地的黑曜岩與玻隕石之差異。C 與 D 圖中清楚可見黑曜岩與玻隕石大致可分類出來（B 左與 D 上明顯分群者為四個產地的澳亞群玻隕石）。

Fig. 5. A 3D scatter plot of component scores for the calibration set data of the natural glass classification model is shown in figures. A to D are the same plot but rotated at different angles, it is possible to observe more clearly the differences between obsidian and tektites from different origins. In figures C and D, it is evident that obsidian and tektites can be roughly distinguished (the clearly separated clusters in B left and D upper are the Australasian tektites from four different origins).

應用拉曼光譜於鈣榴石群化學成份之分析

黃怡禎¹、李佩倫^{2*}、龔慧貞³、鄭文昕⁴、陳君榮⁵

¹ 江西應用科技學院光華寶石與藝術設計學院

² 國立嘉義大學數位學習設計與管理學系

³ 國立成功大學地球科學系

⁴ 中央地質調查所

⁵ 國立自然科學博物館

*通訊作者 E-mail: peilun@mail.ncyu.edu.tw

摘要

石榴子石是常見的寶石礦物，在地質上也是變質作用的指標礦物之一，此族群不管在顏色、化學成分或物理特性上的性質也顯示出明顯的差異，一般其化學式可表示為 $X_3Y_2(SiO_4)_3$ ，其中 X 表價數為+2 的金屬離子（主要有 Mg^{+2} 、 Fe^{+2} 、 Mn^{+2} 和 Ca^{+2} ）；Y 表+3 價的金屬離子（主要有 Al^{+3} 、 Fe^{+3} 、 Cr^{+3} ）。依化學成分可分為兩大系列：鐵鋁榴石-鎂鋁榴石-錳鋁榴石系列（鋁榴石群、Pyralspite）及鈣鋁榴石-鈣鐵榴石-鈣鉻榴石系列（鈣榴石群、Ugrandite）。在寶石鑑定上，由於此系列的礦物具同晶體結構，且顏色多元，因此無法由顏色及晶體外觀直接推測所含化學成份，但若為量測其化學組成，往往需進行破壞性檢測，故在寶石鑑定上非破壞性的化學成份檢測方法之建立是需要的。因此本研究針對鈣鋁/鐵榴石固溶體系列的天然寶石級單晶石榴子石進行拉曼光譜測量，並採用能譜儀（EDS）對其進行相對應的化學成分分析，並將此固溶體系列所得之拉曼光譜各振動模的波數（ ν ）與其相對應的化學成分（x）繪製及計算其線性函數關係，並以 dv/dx 線性關係推測出各端成份石榴子石的振動模之數值，以建置石榴子石之每個拉曼光譜振動模的波數與化學成份的線性函數，此將可提供未來鑑定未知成份的石榴子石時，藉由拉曼光譜所測得的各振動模的波譜及波數，代入函數後，將可提供可能的化學組成範圍。本研究經由已知化學組成的標本之盲試，顯示本函數所計算出之化學成份組成與已知成份的誤差值在 10% 以內，顯示此方法具可信度、在鑑定成份流程上相對簡易且具非破壞性之優勢，故十分適合應用在測定石榴子石寶石晶體的化學組成之方法之一。

關鍵字：石榴子石、拉曼光譜、固溶體、化學組成

Application of Raman Microscopy for Analyzing the Chemical Composition of Ugrandite

Eugene Huang¹, Pei-Lun Lee^{2*}, Jennifer Kung³, Wen-Hsin Cheng⁴, Chung-Jung Chen⁵

¹Guanghua Institute of Gemmology and Mineral Resources, Jiangxi University of Applied Sciences

²Department of E-learning Design and Management, National Chiayi University

³Department of Earth Sciences, National Cheng-Kung University

⁴Central Geological Survey, Ministry of Economic Affairs

⁵National Museum of Natural Science

*Corresponding author, E-mail: peilun@mail.ncyu.edu.tw

Abstract

Garnet is one of the most commonly found and widespread distributed mineral among all gemstones. Garnets of gemstone species show large variation in color, composition and physical properties. The chemical formula of garnets can be expressed as $X_3Y_2(\text{SiO}_4)_3$, where X stands for metallic ion with valence +2 (mainly Mg^{+2} , Fe^{+2} , Mn^{+2} and Ca^{+2}); Y stands for metallic ion with valence +3 (mainly Al^{+3} , Fe^{+3} and Cr^{+3}). Garnet group minerals can be classified as two branches according to their differences in chemical composition as: Almandine-pyrope-spessartine series (called pyrospite, or Al-garnet); Grossular-andradite-uvarovite series (called ugrandite or Ca-garnet). In this research, The Raman spectra of natural gem-quality single-crystal silicate garnets of grossular-andradite solid solution series will be measured and energy-dispersive spectrometer (EDS) is applied for corresponding chemical composition analysis of each specimen in this study. We found that most of the wavenumber of Raman modes show linear relationship with major component of garnet. The wavenumber of each vibrational mode as a function of composition, dv/dx , makes it possible to provide reliable chemical composition range for unknown silicate garnet. We have also established the ideal Raman modes positions of the end-member silicate garnets on the basis of the present systematic investigation on garnets. Our results can provide reliable way of determining mineral species of garnet group, especially pyrope-almandine and grossular-andradite series. It is promising that Raman spectroscopic method can be adopted in all gemological laboratories for the quick and non-destructive determination of mineral species of garnets and other gemstones with solid solution variety.

Keywords: Garnet, Raman Microscopy, Solid Solution, Chemical Composition

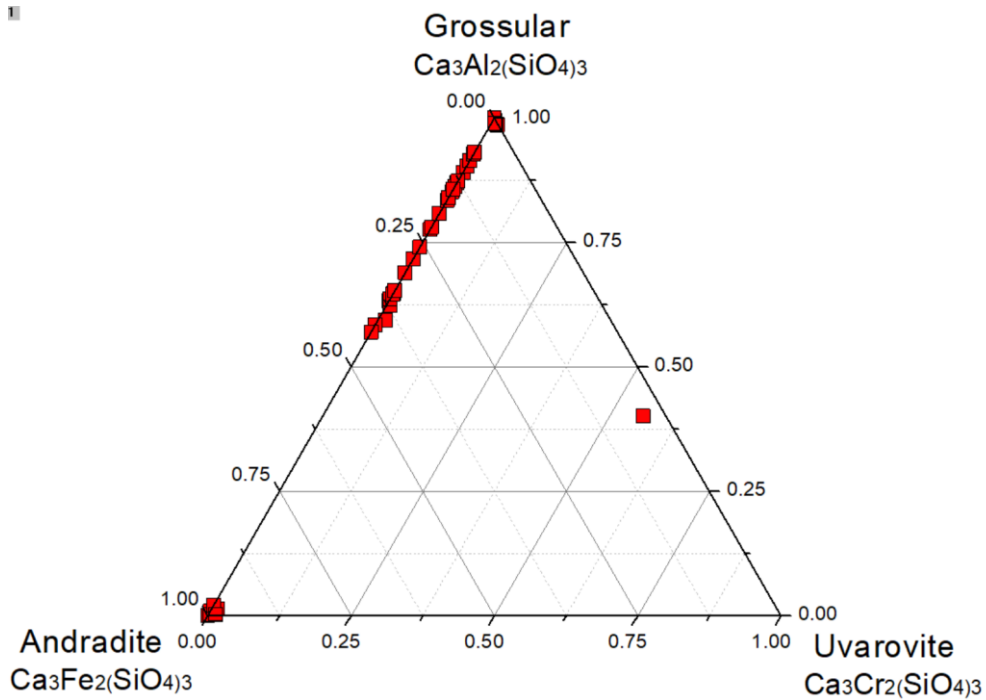


圖 1、本研究鈣榴石群礦物標本之化學成份分佈圖

Fig. 1. Grossular-andradite-uvarovite ternary diagram showing compositions of ugrandite samples analyzed in this study

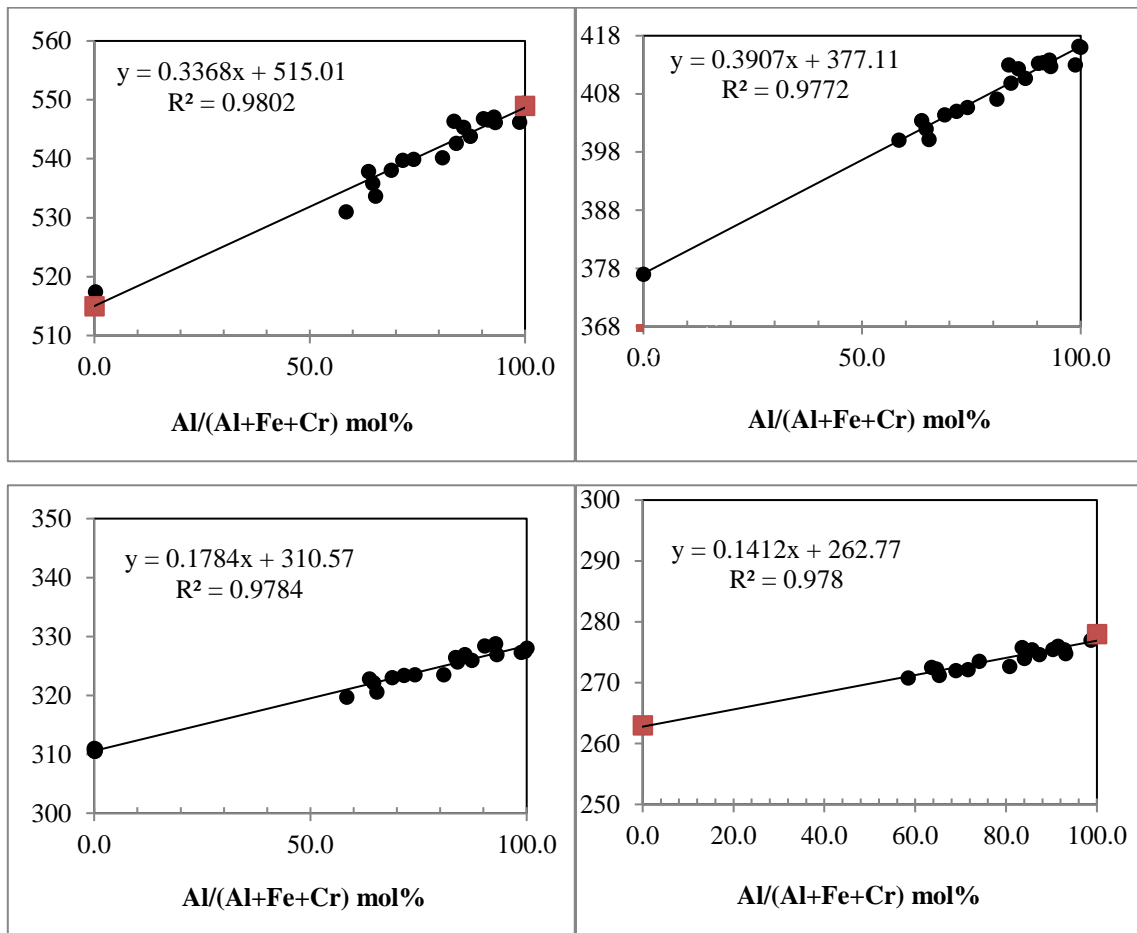


圖 2、鈣榴石群礦物之拉曼光譜波數隨化學成份組成之變化圖。

Fig. 2. The wavenumber shifts versus Al/(Al+Fe+Cr) plots of 4 selected Raman bands of ugrandite specimens, showing remarkable dv/dx linear relationship. Exact wavenumber of end-member grossular and andradite can be determined by the extrapolation of linear relation. (●: this study; ■: wavenumber be determined by the extrapolation of linear relation)

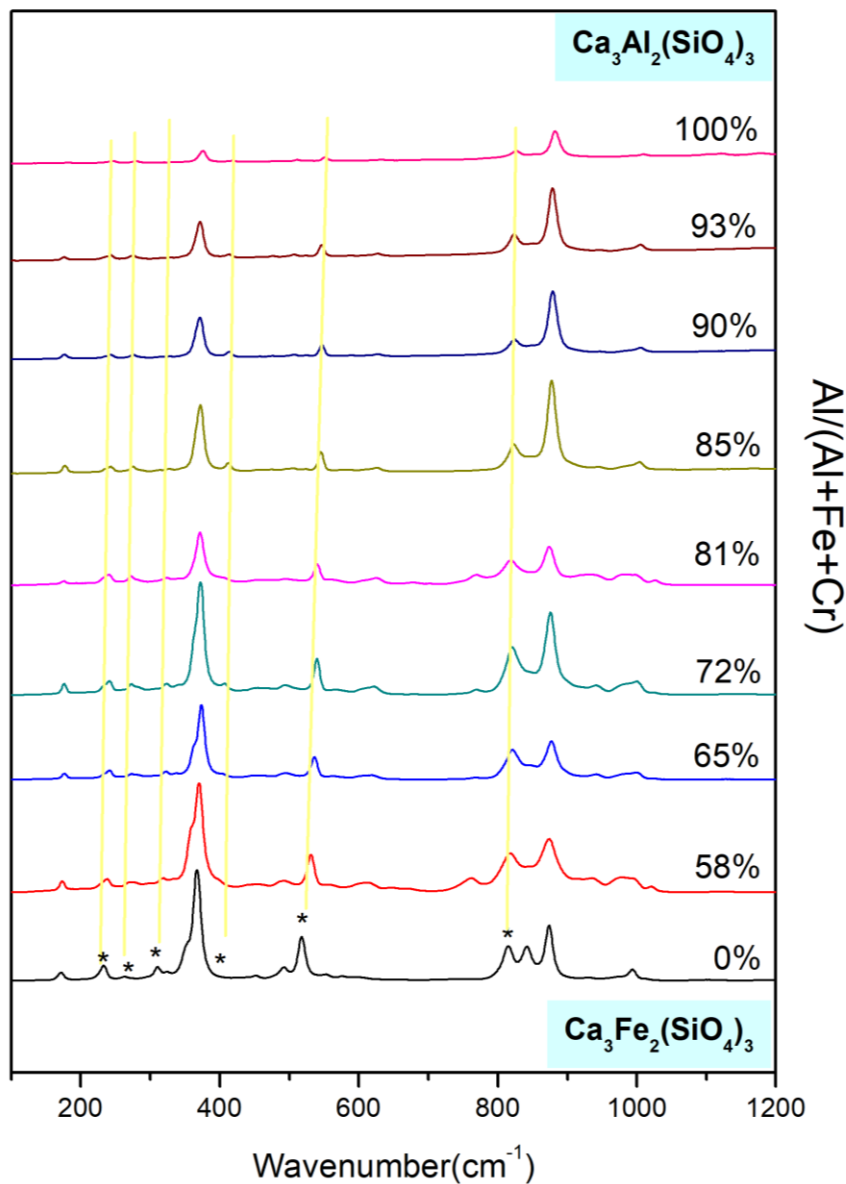


圖 3、鈣榴石群礦物之拉曼光譜隨化學成份組成之變化圖。

「*」：表適合用來測試成份之譜線位置。

Fig. 3. Superimposed Raman spectra of samples in grossular-andradite binary showing with the shift of various Raman modes with different Al³⁺/(Al³⁺+Fe³⁺+Cr³⁺) Mole%. Yellow lines indicate trend of shift of 6 selected peaks at approximately 235cm⁻¹, 265cm⁻¹, 311cm⁻¹, 515cm⁻¹ and 815cm⁻¹.

用地球化學指標鑑定祖母綠的來源

宋聖榮

國立臺灣大學地質科學系

E-mail : srsong@ntu.edu.tw

摘要

決定一顆寶石的價值常用 4C-顏色、大小（克拉）、淨度和切割等來判定，但有些寶石的產地也會影響其價格，如來自於哥倫比亞的祖母綠、特別是產於木佐的，其價格就比其他地方產的高出許多。故鑑定祖母綠的產地一直是研究和買賣祖母綠非常重視的課題。從地質的觀點來看，地球化學特性是鑑定一種礦物岩石的來源、產狀和成因最有效的工具，尤其是所含微量元素種類和同位素比率是最有用的鑑別方法。祖母綠的產狀和成因主要有兩種：含高鉍元素熱液沉澱於沉積岩中的礦脈和花崗岩漿侵入變質岩中所形成的偉晶岩脈中，前者以哥倫比亞所產的祖母綠為代表，後者則是產於大部分國家的祖母綠。本研究擬用地球化學的分析資料，利用微量元素的鑑別圖，來區分祖母綠的產地，尤其是區分出哥倫比亞的祖母綠。

關鍵字：哥倫比亞、祖母綠、地球化學、微量元素、鑑別圖

Identifying the Emerald's place of Origin by Geochemical Discrimination Diagram

Sheng-Rong Song

Department of Geosciences, National Taiwan University

E-mail: srsong@ntu.edu.tw

Abstract

The price of a gem is determined by the 4-C properties, such as color, weight (carat) 、 clarity and cut, etc. However, some gems are also influenced by the place of origin, such as emerald from Columbia, especially from the Muzo area, which its price would be much higher than ones from other countries. Therefore, identifying the emerald origin is a very important topic for researchers and businesses. From the geological point of view, geochemical characteristic, especially the trace elements and isotopic ratio of rocks and minerals, is a useful tool and method for discriminating the source, occurrence and origin of emerald. Generally, two occurrences of emerald can be recognized in the world. One is the Be-rich thermal fluids precipitated as veins in sedimentary formation, while the other is granitic magma intruded into metamorphic terrane as pegmatitic dikes. The former is dominated from the Columbia's emerald, while the latter is distributed in other countries of the world. This study uses the geochemical database to build up the trace element discrimination diagrams as tool for determining the source of emerald, especially the Columbia's one.

Keywords: Columbia, Emerald, Geochemistry, Trace elements, Discrimination diagrams

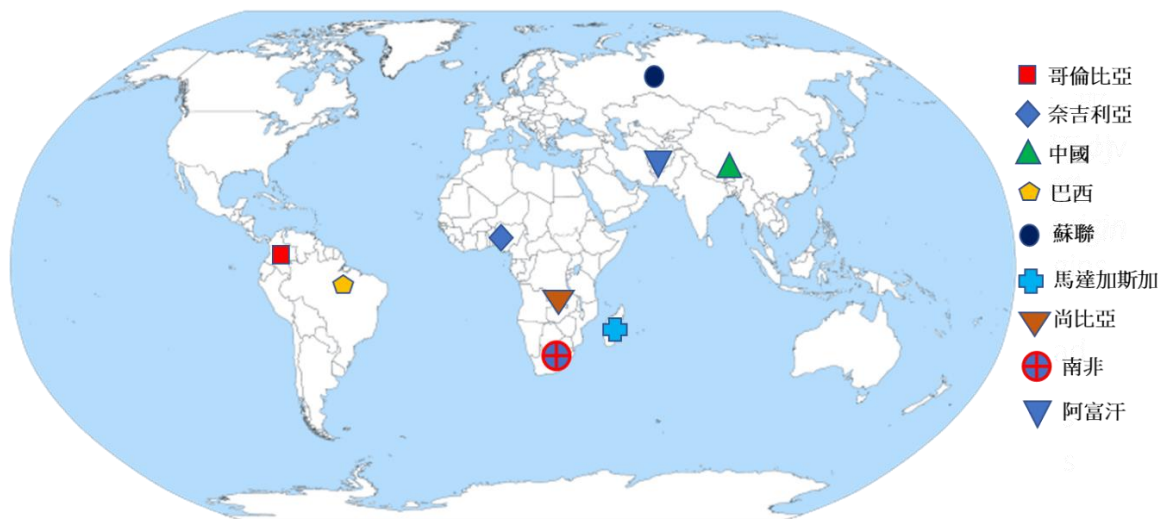


圖 1、世界主要祖母綠出產國家的分布。

Fig. 1. Emerald distributions of main countries in the world.

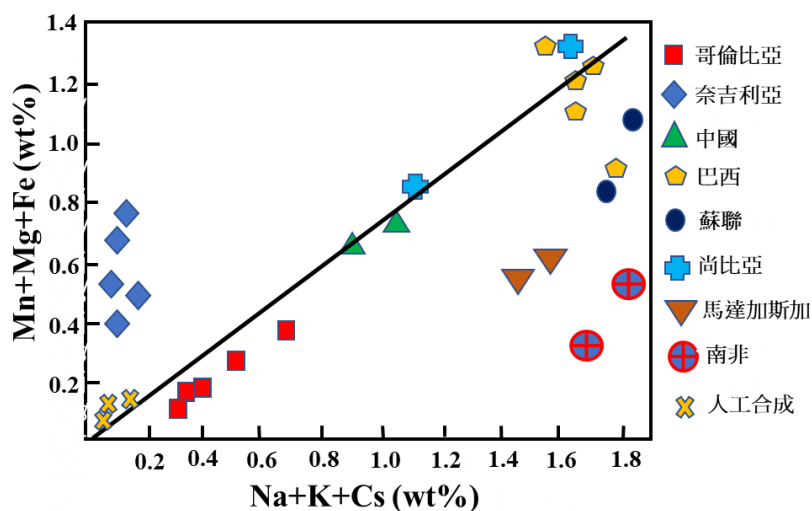


圖 2、祖母綠 Na+K+Cs vs. Mn+Mg+Fe 鑑別圖。

Fig. 2. Discrimination diagram of Na+K+Cs vs. Mn+Mg+Fe for emeralds.

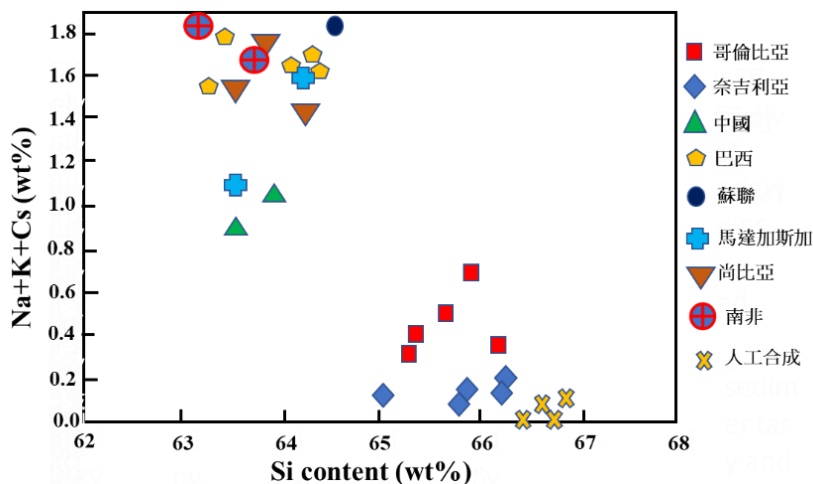


圖 3、祖母綠 Si content vs. Na+K+Cs 鑑別圖。

Fig. 3. Discrimination diagram of Si content vs. Na+K+Cs for emeralds.

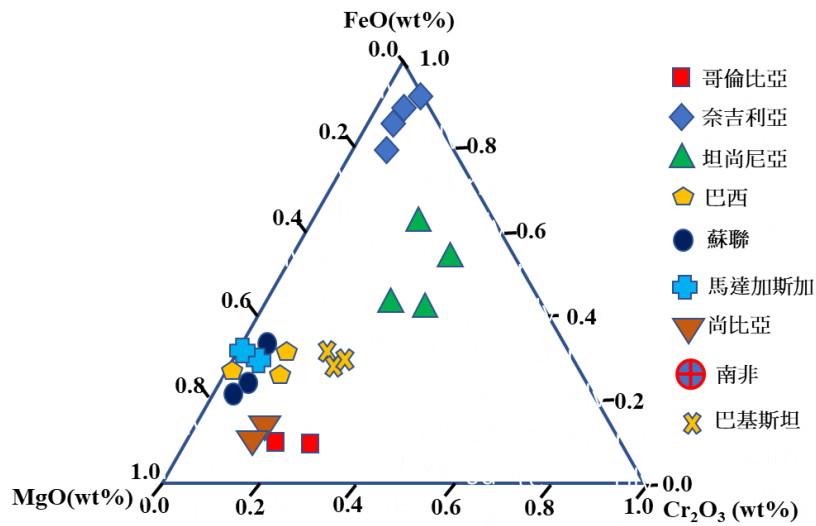


圖 4、祖母綠 FeO vs, MgO vs. Cr₂O₃ 三相鑑別圖。

Fig. 4. Discrimination diagram of FeO vs, MgO vs. Cr₂O₃ for emeralds.

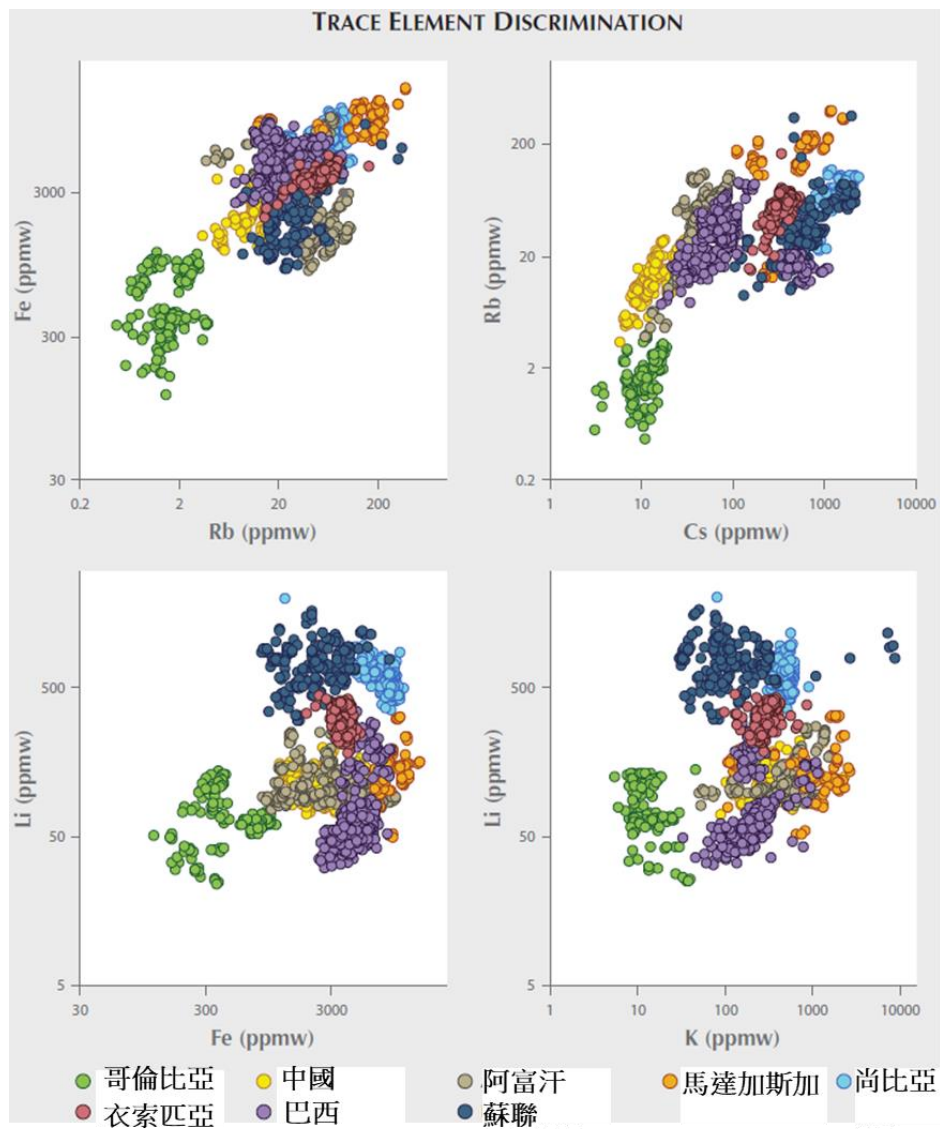


圖 5、祖母綠微量元素鑑別圖 (Saeseaw, et al., 2019)。

Fig. 5. Discrimination diagram of trace elements for emeralds (Saeseaw, et al., 2019).

拉曼光譜與密度泛函理論計算在紅珊瑚色素鑑別研究中的應用

陳超洋¹、沈錫田^{1*}

¹ 中國地質大學（武漢）珠寶學院

*通訊作者 E-mail: ahshen1@live.com

摘要

紅珊瑚是一種歷史悠久且廣受歡迎的有機寶石，其顏色直接影響其經濟價值。目前關於紅珊瑚的色素研究仍有一定爭議，主要觀點有兩種：類胡蘿蔔素（角黃素）與脫甲基化的多烯。其中紅珊瑚中的色素為角黃素這一觀點是通過分析化學的方法（色素提取後通過高效液相色譜-質譜聯用技術分析）得出的，脫甲基化的多烯色素這一觀點是根據紅珊瑚拉曼光譜的特點推測的。在實驗方面，拉曼光譜技術是一種常用的有機物分析表徵手段。在理論方面，密度泛函理論（Density Functional Theory，簡稱 DFT）計算可以用模擬分子的拉曼光譜並研究分子的振動模式。基於現有的研究背景，我們收集了不同品種的顏色深淺不同的紅珊瑚樣品，測試了這些樣品的拉曼光譜，並運用密度泛函理論模擬了可能的色素分子（不同鏈長的多烯鏈、角黃素、脫甲基化的角黃素）的理論拉曼光譜。結果發現，在紅珊瑚的拉曼光譜中主要存在位於 1516、1298、1181、1128、1088、1017 cm^{-1} 處的拉曼峰，其中 1088 cm^{-1} 歸屬於方解石，其餘這些拉曼峰的強度與紅珊瑚的紅色濃度呈現正相關關係，推測為色素峰，同時這些色素峰呈現出多烯類色素的特點。通過將紅珊瑚的實驗拉曼光譜與可能色素分子的理論模擬拉曼光譜進行對比後發現：紅珊瑚中的色素是含有 11 個 C=C 雙鍵多烯類色素，很可能是類胡蘿蔔素（角黃素）脫甲基後形成的色素。對於生物礦物類的有機寶石，通過分析化學的方法提取色素與鑑定色素可能較為困難，可以通過拉曼光譜學技術與密度泛函理論模擬來研究其中的色素成分，為色素的精準鑑定提供更多的理論依據。

關鍵字：紅珊瑚、色素、類胡蘿蔔素、拉曼光譜、密度泛函理論

Application of Raman Spectroscopy and DFT Calculation in the Identification of Red Coral Pigments

Chao-yang Chen¹, Andy Hsien Shen^{1*}

¹Gemmological Institute, China University of Geosciences, Wuhan

*Corresponding author, E-mail: ahshen1@live.com

Abstract

Red coral is a historical and popular organic gemstone, and its color directly affects its economic value. There are still some controversial studies on the pigmentation of red coral, with two main views: carotenoids (canthaxanthin) and demethylated polyenes. Among them, the view that the pigment is carotenoid is obtained by analytical chemistry (pigment extraction and analysis by high performance liquid chromatography-mass spectrometry), and the view that the pigment is demethylated polyene is speculated based on the characteristics of Raman spectra of red corals. On the experimental side, Raman spectroscopy is a commonly used tool for the analytical characterization of organic matter. On the theoretical side, Density Functional Theory (DFT) calculations can be used to simulate the Raman spectra of molecules and to study the vibrational modes of molecules. Based on the existing research, we collected red coral samples of different species with different color shades, tested the Raman spectra of these samples, and simulated the theoretical Raman spectra of possible pigment molecules (polyene chains, canthaxanthin, demethylated canthaxanthin) by DFT calculation. It was found that Raman peaks located at 1516, 1298, 1181, 1128, 1088, 1017 cm^{-1} were mainly present in the Raman spectra of red coral, among which 1088 cm^{-1} was assigned to calcite, and the intensity of other peaks showed a positive correlation with the red concentration of coral, which were presumed to be pigment peaks. These peaks also showed the characteristics of polyene pigments. By comparing the experimental Raman spectra of red coral with the theoretical Raman spectra of possible pigment molecules, it was found that the pigment in red coral is a polyene containing 11 C=C double bond, most likely formed by demethylation of carotenoid (canthaxanthin). For organic gemstones of biomineral origin, it may be difficult to extract and identify pigments by analytical chemistry, and the pigments can be studied by Raman spectroscopy and DFT calculations to provide more theoretical basis for accurate pigment identification.

Keywords: red coral, pigment, carotenoid, Raman spectroscopy, DFT calculation



圖 1、不同種類的紅珊瑚樣品：沙丁紅珊瑚（SD-01 與 SD-02）、阿卡紅珊瑚（AK-01 與 AK-02）與 MOMO 紅珊瑚（MM-01 與 MM-02）

Fig. 1. Different varieties of red coral samples: Sardinian red coral (SD-01 and SD-02), Acropora coral (AK-01 and AK-02), and MOMO coral (MM-01 and MM-02).

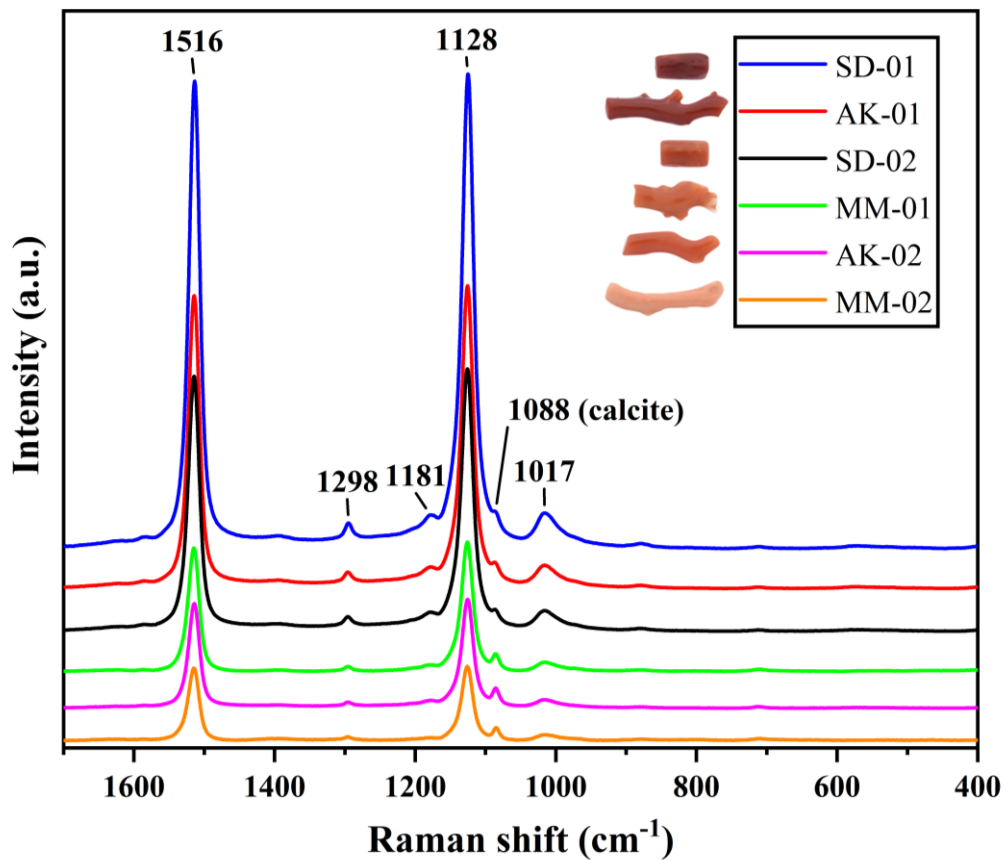


圖 2、紅珊瑚樣品的拉曼光譜

Fig. 2. Measured Raman spectra of different red corals.

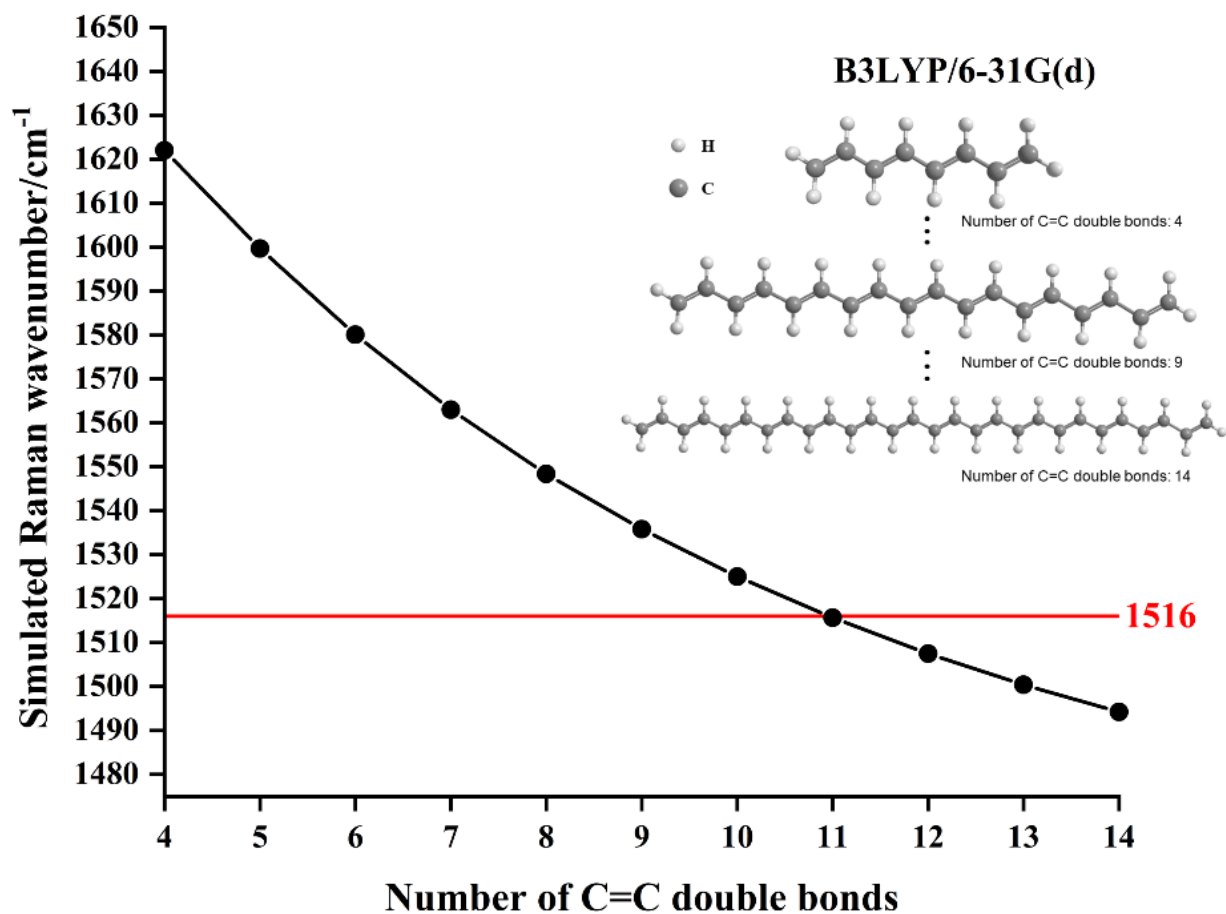


圖 3、不同鏈長多烯的 C=C 雙鍵數目與 DFT 模擬的 C=C 雙鍵伸縮振動的拉曼位移的關係

Fig. 3. The relationship between the number of C=C double bonds in polyenes with different chain lengths and the Raman shift of C=C double bond stretching vibration simulated by DFT

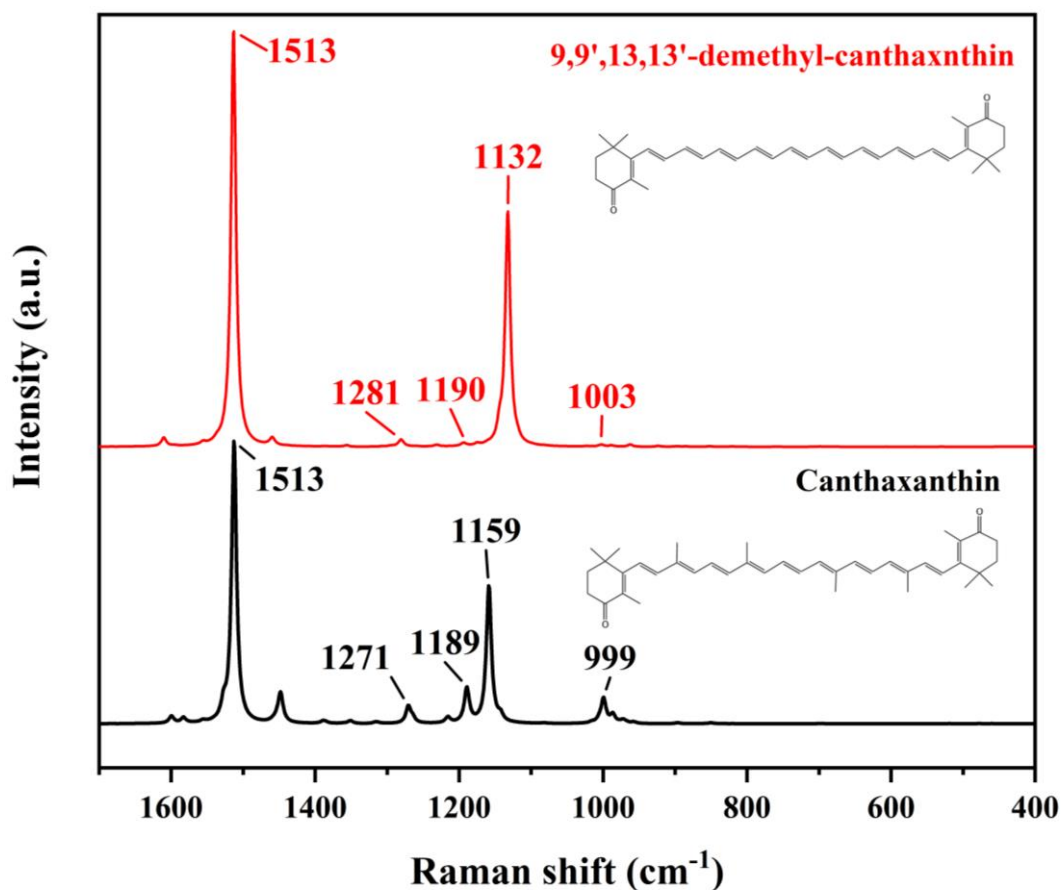


圖 4、DFT 模擬的角黃素與 9,9',13,13'-脫甲基-角黃素的理論拉曼光譜

Fig. 4. Theoretical Raman spectra of lutein and 9,9',13,13'-demethyl-lutein simulated by DFT.

表 1、紅珊瑚的主要實驗拉曼譜峰與角黃素和脫甲基角黃素的主要理論拉曼譜峰對比

Table 1. Comparison of the main experimental Raman peaks of red coral with the main theoretical Raman peaks of lutein and demethyl-lutein calculated by DFT

| | 紅珊瑚實驗拉曼峰位 /cm ⁻¹ | 角黃素理論拉曼峰位 /cm ⁻¹ | 脫甲基角黃素理論拉曼峰位 /cm ⁻¹ |
|--------|--------------------------------|--------------------------------|-----------------------------------|
| C=C 伸縮 | 1516 | 1513 | 1513 |
| C-H 搖擺 | 1298 | 1271 | 1281 |
| C-C 伸縮 | 1181 | 1189 | 1190 |
| C-C 伸縮 | 1128 | 1159 | 1132 |
| 甲基搖擺 | 1017 | 999 | 1003 |